An investigation of the performance of and the flow of solids and air in a vertical shaft impactor

Damian Patrick Mapletoft Leonard

An Investigation of the Performance of and the Flow of Solids and Air in a Vertical Shaft Impactor

D. P. M. Leonard, B.Sc.

Thesis submitted for the degree of Master of Science

Year of submission: 1991

ABSTRACT

The operation of the Breakring vertical shaft impactor was investigated mathematically and experimentally. In particular, the performance of the crusher, the action of solids and air in the impeller and the mechanism responsible for the localised abrasion of the impeller wear parts were investigated.

Computer programs were developed, which modelled the performance of the Breakring for impellers having simple, idealised wear part profiles. Contour plots were produced, which illustrated the dependence of impeller power, absolute particle exit speed and anvil angle for normal impact on the wear part sweep angle and the coefficient of friction between the feed material and the wear part. The significance of the contours was investigated.

A computer program was developed, which modelled the action of a single particle in the Breakring impeller for wear parts having various complex profiles. The results indicated that the cause of the localised wear part abrasion was the reattachment of feed material to the wear part, following separation at the downstream end of the depression caused by action of material after entry to the impeller. The accuracy of the results was confirmed by the profiles of abraded wear parts and various other factors.

A full-scale model impeller was constructed. The flow of air in the model and, following failure of the model, the flow of air and solids in a prototype impeller were investigated by a surface flow visualisation technique and high speed cinematography. The results neither verified the wear-mechanism outlined above nor indicated any other wear-mechanism.

It was concluded that the wear mechanism indicated by the mathematical modelling was accurate and that there is no indication of abrasion by airborne fines.

An Investigation of the Performance of and the Flow of Solids and Air in a Vertical Shaft Impactor

One Volume

by

Damian Patrick Mapletoft Leonard, B.Sc.

Thesis submitted for the degree of Master of Science at the University of Durham

School of Engineering and Applied Science

Year of submission: 1991

CONTENTS PAGE

LIST OF FIGURES PAGE

STATEMENT OF COPYRIGHT

With the exception of the following, the material contained in the thesis is the original work of the author. The analysis described in Section 2.1.1 is the work of Dr. J. M. Wilson. The computer program described in Section 2.2.1 is derived from a program written by Dr. Wilson. No material in the thesis has previously been submitted for a degree at the University of Durham or any other university.

LIST OF SYMBOLS

a	acceleration of particle
b	wear part chord length
c	radius to anvil centre
d	radius to upstream end of wear part
e	radius to downstream end of wear part
f	frictional force on particle
h	radius of curvature of wear part
m	impeller mass flow rate
n	normal force on particle
P	impeller power
Q	radius to particle position
R	radius to segment midpoint
δs	length of wear part segment
s	distance of particle from upstream end of wear part
T	time
V,v	speed of particle
X,x	X,x - coordinate of point

Y,y Y,y - coordinate of point

α angle between segment tangent and radius to segment midpoint

β anvil angle for normal impact

γ half angle of wear part arc

ϵ angle between radius to segment midpoint and x-axis

Θ wear part sweep angle

μ coefficient of friction between particle and wear part

ρ angle between segment tangent and x-axis

Σ,σ angle between radius to particle position and X,x-axis

φ angle between direction of absolute exit velocity and direction of wear part chord at instant of exit

χ reattachment angle

ψ angle between radius to anvil centre and direction of wear part chord at instant of exit

ω angular speed of impeller

N.B. 1. Upper case characters indicate absolute quantities. Lower case characters indicate quantities relative to impeller.

2. All radii, other than h, the radius of curvature of the wear part, are measured from the centre of rotation of the impeller.

SUBSCRIPTS

i	condition at i^{th} segment
k	condition at k^{th} segment
X	X-component
Y	Y-component
1	condition at upstream end of wear part
o	condition at downstream end of wear part
c	circumferential component

1. INTRODUCTION

Construction aggregates are generally obtained from two sources, gravel pits and rock quarries. Gravel pits contain a mixture of sand and gravel which is recovered, in dry deposits, by shovel, dragline or bulldozer and, in wet deposits, by dragline or dredging. Rock quarries contain massive rock, which is separated by blasting (Hewitt-Robins, undated).

Prior to use the raw materials are processed in crushing plant, typically comprising a series of crushers with facilities for cleaning and screening and a closed circuit for recrushing oversized product. Crushers are classed as primary, secondary or tertiary, according to their feed size and role in the plant. Primary crushers accept massive chunks of feed. They are not intended to prepare material to meet specification but only to reduce it to a more workable size. Tertiary crushers are used for the final reduction and shaping of material. Secondary crushers come in between. Most gravel crushing operations employ only tertiary crushers (Hewitt-Robins, undated). There are four fundamental mechanisms by which crushing is accomplished. These are pressure, impact, shear and attrition (Hewitt-Robins, undated). There are many types of crusher, each employing one or more of these mechanisms (Höffl, 1985).

This report concerns a type of tertiary impact crusher called vertical shaft impactor or VSI (Garland, 1977; Höffl, 1985). A typical VSI is shown in Figure 1. A horizontal disc (1) is mounted centrally on a vertical drive shaft (2). The upper face of the disc is equipped with a central distributor cone (3) and a number of re-

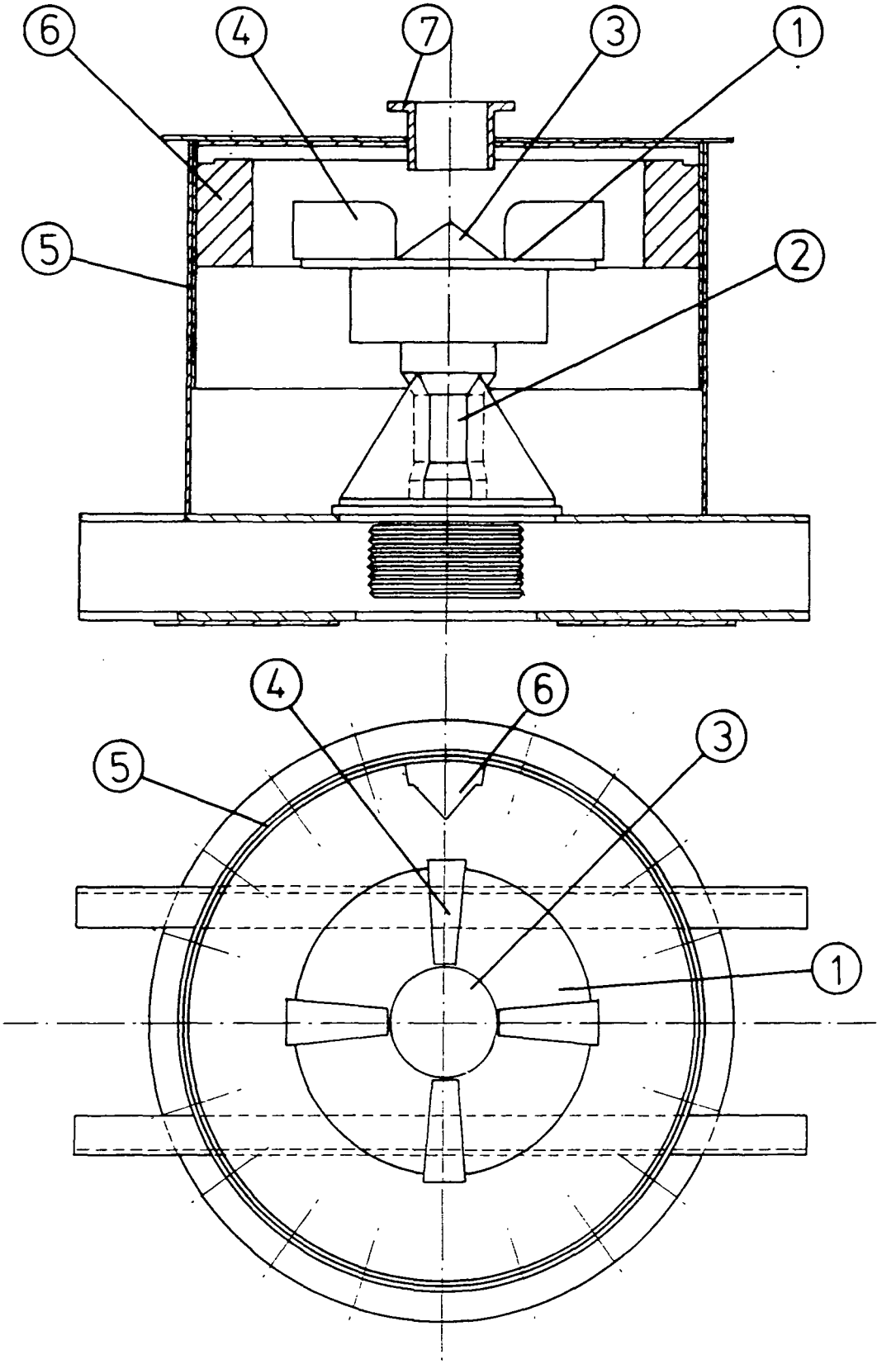

Figure 1

Vertical Shaft Impactor

placeable shoes (4). This impeller assembly is housed in an armoured cylindrical chamber (5), having an inclined base with a discharge opening at its lower end. Surrounding the impeller is an array of anvils (6). A horizontal lid containing a stationary feed tube (7) covers the chamber.

The impeller is driven at between 700 and 1500 r.p.m. Material is fed into the feed tube and falls onto the distributor cone of the impeller. Some horizontal motion is imparted to the material, which enters the channels between the impeller shoes and is accelerated centrifugally along the leading faces of the shoes. The material leaves the impeller at high speed and smashes against the anvils. The fragments fall to the base of chamber and leave via the discharge opening. After an operating period of between 20 and 200 hours, the impeller shoes become worn and must be replaced.

The VSI has two major advantages. It generates a well shaped product. On impact, the feed particles tend to fragment along their natural planes of weakness, these being approximately perpendicular to each other. A cubical product thus results (Harvey, undated). It also produces a well graded output. All product sizes, from smallest to largest, are present in similar amounts (Hewitt-Robins, undated). These characteristics are ideal in a tertiary crusher.

The major disadvantage of the VSI is an inability to cope with highly abrasive materials, since the impeller shoes are designed for both toughness and hardness and excel in neither (Garland, 1983). One machine which does not suffer so severely from this weakness is the autogenous or stone-on-stone crusher (Bartley, 1989; Hill, 1988; Huwald, 1987; Müller and Weigel, 1988). In its basic form, the autogenous crusher possesses two features not

found on other VSIs. A forward facing tip is affixed to the downstream end of each impeller shoe. A rock bed builds up behind the tip, lining the shoe and protecting it from abrasion. A shelf mounted beneath the anvil array collects comminuted rock which piles up against the anvils and shields them from impact damage.

The autogenous crusher's usefulness is strictly limited by a number of new problems. These are inefficient impact at the anvils, leading to a low size reduction (Huwald, 1987), rock on rock abrasion, leading to a large proportion of (generally undesirable) fines in the product (Hill, 1987), high rock on rock friction, leading to a large power consumption (Hill, 1987), and the impeditive spiral profile of the impeller rock bed, defined by the angle of repose of material under the influence of centrifugal force.

Impact Technology Ltd. of Stockton, Cleveland has developed a VSI called the Breakring (Garland, 1977; Garland, 1983) which is claimed to process hard and abrasive materials effectively. The stator of the Breakring is similar to that of other VSIs. The impeller, which is shown in two- and six- port configurations in Figure 2, is covered to form an enclosed chamber, the interior of which is lined with replaceable wear parts, by a lid, containing, at its centre, a short feed tube known as the breakring. The purpose of the breakring is to impart some rotational speed to the feed material before entry to the impeller. This action is claimed to have two effects, both of which lead to more economical crushing operation. These are a directed and energy efficient motion of the feed material, from the instant it enters the breakring, and a reduced impact between the feed particles and the impeller interior, permitting the use of less tough but harder wear part materials, which wear more slowly and often offer less resistance to the

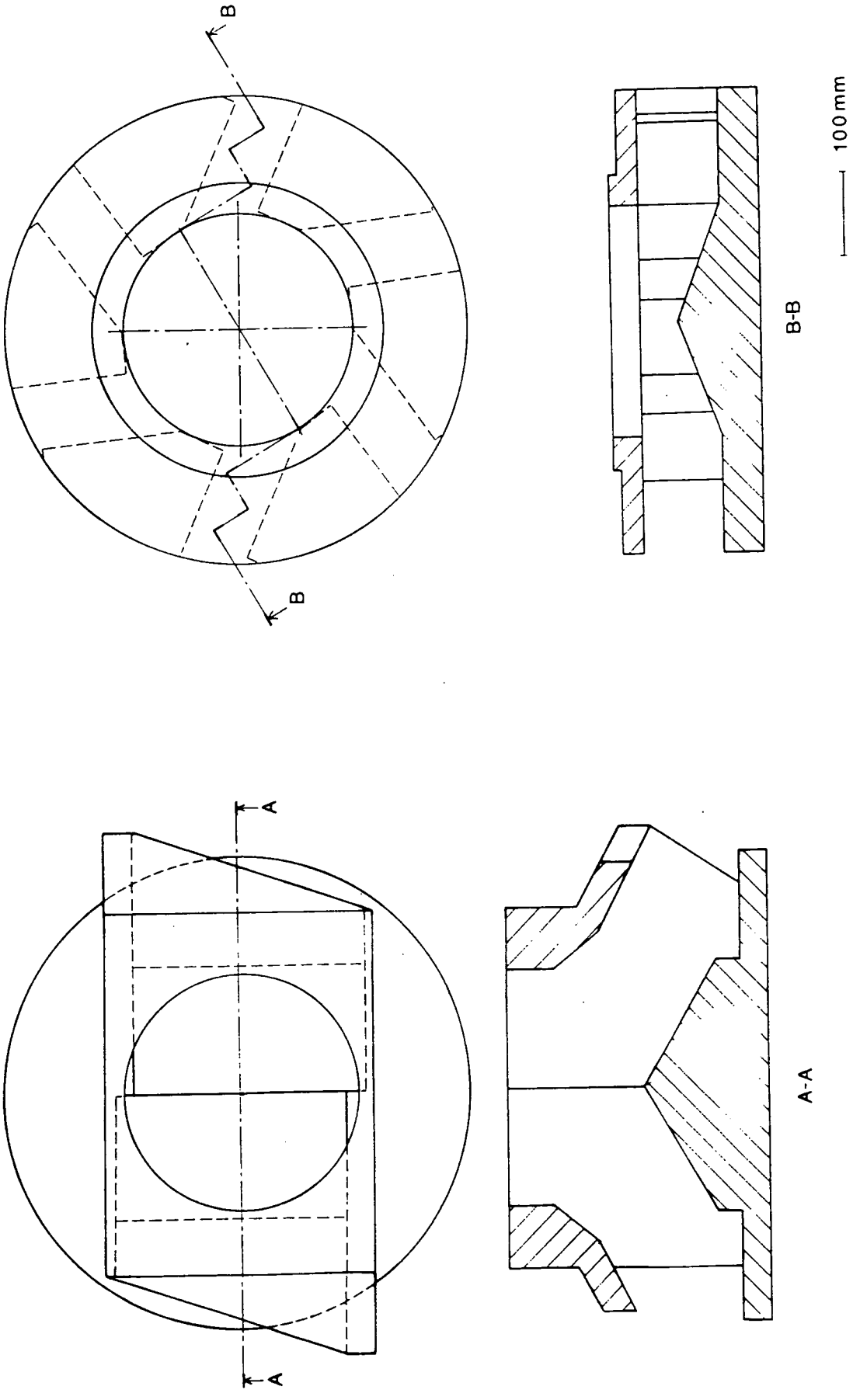

Figure 2

Breakring Impeller (two- and six-port configurations)

N.B. Direction of rotation clockwise

sliding motion of the particles. Impact Technology supplies ceramic and chrome-iron wear parts.

Centrifugal force causes the feed particles to adhere to the breakring and, in extreme cases, choke the flow entirely. This condition is prevented by lowering the stationary feed tube into the breakring, so as to reduce the effective length of the latter. The optimum position of the stationary feed tube is that at which the breakring is densely packed but still passing material, so that maximum energy transfer occurs. It depends on the feed material, the throughput and the impeller speed and is determined experimentally.

In some early trials, the wear parts lining the forward facing side walls in both two- and six- port impellers wore rapidly and unevenly. A set of worn two- port wear parts is shown in Figure 25. The long shallow upstream depression and the short deep downstream depression are typical. Similar patterns were observed on the worn wear parts of six- port impellers. The abrasion was especially severe when the feed material contained a large fraction of fines. To the date of writing, the problem has been avoided by the use of shorter wear parts in a modified six- port impeller. The two- port impeller is employed only in less demanding applications. This wear problem has not been reported previously.

The present research was completed under contract with Impact Technology Ltd. It had three main objectives.

1. Analysis and computation of the action and performance of the Breakring.

2. Experimental modelling of Breakring operation.

3. Investigation of the mechanism responsible for

the localised abrasion of the wear parts.

To meet these ends, the following program was undertaken.

1. Development of FORTRAN computer programs to produce contour plots characterising Breakring performance for impellers having simple, idealised wear part profiles.

2. Development of FORTRAN computer programs to model the action of a single particle in the Breakring impeller, having wear parts of any specified profile.

3a. Design, manufacture and installation of a full scale, variable geometry model impeller for experimental investigation of the flow of airborne fines.

3b. Employment of a surface flow visualisation technique to study the air flow in the vicinity of the impeller wear parts.

3c. Photography of the flow of material within the impeller.

Following the disintegration of the model impeller, parts 3b and 3c were completed on Impact Technology's diesel driven demonstration crusher at Eaglescliffe.

2. COMPUTATION OF BREAKRING PERFORMANCE

2.1 Analysis

2.1.1 Impeller having flat wear parts

The action of a single particle in the Breakring impeller is analysed. The analysis is valid for an impeller having flat wear parts. Since the motion of material in the impeller is approximately horizontal, a two-dimensional model is considered. The following refers to the arrangement shown in Figure 3. The particle is treated as a unit mass subjected only to inertia and frictional and normal forces, f and n, at the wear part surface. The frictional and normal forces are related by equation (1)

$$f = \mu n \quad \ldots (1)$$

where μ is the constant coefficient of friction between the particle and the wear part. The impeller rotates anticlockwise at angular speed ω. The particle makes contact with the upstream end of an impeller side wear part at radius d from the centre of rotation and, in general, slides some distance along the wear part towards the exit port. The wear part is inclined at sweep angle θ to the radius d. At any distance s from the upstream end of the wear part, the particle has speed v and acceleration a relative to the wear part. From equilibrium of forces, it can be shown that

$$f = \omega^2 (d \cos \theta + s) - a \quad \ldots (2)$$

and

$$n = 2\omega v + d\omega^2 \sin \theta \quad \ldots (3)$$

Figure 3

Breakring Two-Dimensional Arrangement:

Flat Impeller Wear Parts

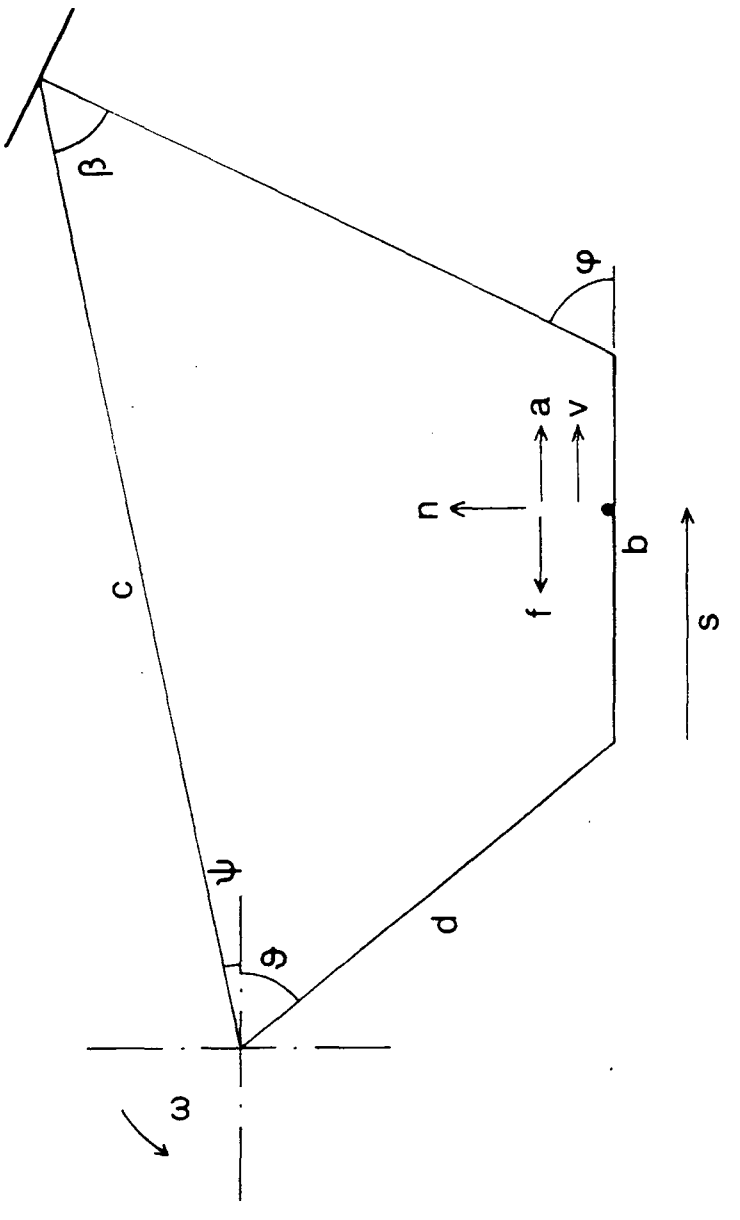

Substitution of equations (2) and (3) in equation (1) leads to

$$a+2\mu\omega v-\omega^2 s = d\omega^2 (\cos\theta-\mu \sin\theta) \ldots (4)$$

Putting

$$a = v\, dv/ds \ldots (5)$$

equation (4) becomes

$$v\,dv/ds+2\mu\omega v-\omega^2 s = d\omega^2 (\cos\theta-\mu \sin\theta) \ldots (6)$$

Solution of equation (6) with $v = v_1$ at $s = o$ yields the relative speed of the particle at any distance from the upstream end of the wear part. In general, at some distance from the upstream end of the wear part, the particle stops, reverses or separates from the wear part surface. Only when the particle slides the whole distance b along the wear part and emerges from the exit port is the impeller considered to function correctly.

The angular momentum of a feed particle is defined as the product of its mass, its radius from the centre of rotation and the circumferential component of its absolute velocity. The impeller torque is given by the rate of change of the angular momentum of the feed material from the upstream end to the downstream end of the wear part. The impeller power is given by the product of the impeller torque and angular speed. Thus

$$P = m\omega^2(b^2+2db\cos\theta + (d/\omega)(v_o - v_1)\sin\theta) \ldots (7)$$

where P is the impeller power, m the impeller mass flow rate and v_o the relative exit speed.

The absolute exit velocity of the particle is equal to the sum of the relative exit velocity and the wear part tip velocity and has components V_{xo} and V_{yo} respectively tangential and normal to the wear part at the instant of exit. Thus,

$$V_{xo} = v_o + d\omega \sin \theta \quad \ldots (8)$$

and

$$V_{yo} = \omega(b + d \cos \theta) \quad \ldots (9)$$

The absolute exit speed V_o and angle φ are given by

$$V_o = (V_{xo}^2 + V_{yo}^2)^{1/2} \quad \ldots (10)$$

and

$$\varphi = \arctan (V_{yo}/V_{xo}) \quad \ldots (11)$$

Time T elapses between exit from the impeller and impact at the anvil. It can be shown that

$$T = \frac{-V_{XO}(d \cos \theta + b) + V_{YO}(d \sin \theta) + \sqrt{(V_{XO}(d \cos \theta + b) - V_{YO} d \sin \theta)^2 - V_O^2((d \cos \theta + b)^2 + (d \sin \theta)^2 - c^2)}}{V_O^2}$$

$$\ldots (12)$$

The radius c from the centre of the impeller to the anvil centre is inclined at angle Ψ to the direction of the wear part at the instant of exit, where

$$\Psi = \arctan ((V_{yo}T - d \sin \theta)/(V_{xo}T + d \cos \theta + b)) \quad \ldots (13)$$

The anvil is inclined at angle β to the circumference through the anvil centre. For normal impact

$$\beta = \varphi - \Psi \quad \ldots (14)$$

This analysis, as those of Sections 2.1.2 and 3.1, is strictly valid only for the Breakring and not for other VSIs, since a controlled initial contact between the feed material and the wear part is assumed.

2.1.2 Impeller having cylindrical wear parts

The analysis of Section 2.1.1 is applied to the more general case of an impeller having cylindrical wear parts. The following refers to the arrangement shown in Figure 4. The length of the wear part along which the particle slides has uniform concave curvature of radius h. s, v and a denote the displacement, speed and acceleration of the particle along the arc, b the chord length and Θ the sweep angle between the wear part chord and the radius d to the upstream end of the wear part. The half angle γ of the arc is given by

$$\gamma = \arcsin (b/(2h)) \quad \ldots (15)$$

By a method similar to that of Section 3.1.1 equation (16) may be derived.

$$v\, dv/ds+\mu v^2/h+2\omega\mu v+\mu\omega^2 h+f1\, \sin\lambda+f2\, \cos\lambda = 0 \ldots (16)$$

where

$$f1 = -\mu\omega^2 d \cos \Theta - \mu\omega^2 b/2 - \omega^2 d \sin \Theta - \omega^2 h \cos$$

$$f2 = \mu\omega^2 d \sin \Theta - \mu\omega^2 h \cos \gamma - \omega^2 d \cos \Theta - \omega^2 b/2$$

$$\lambda = \gamma - s/h$$

Solution of equation (16), with $v = v_1$ at s=o, yields the relative speed of the particle at any distance from

Figure 4

Breakring Two-Dimensional Arrangement:

Cylindrical Impeller Wear Parts

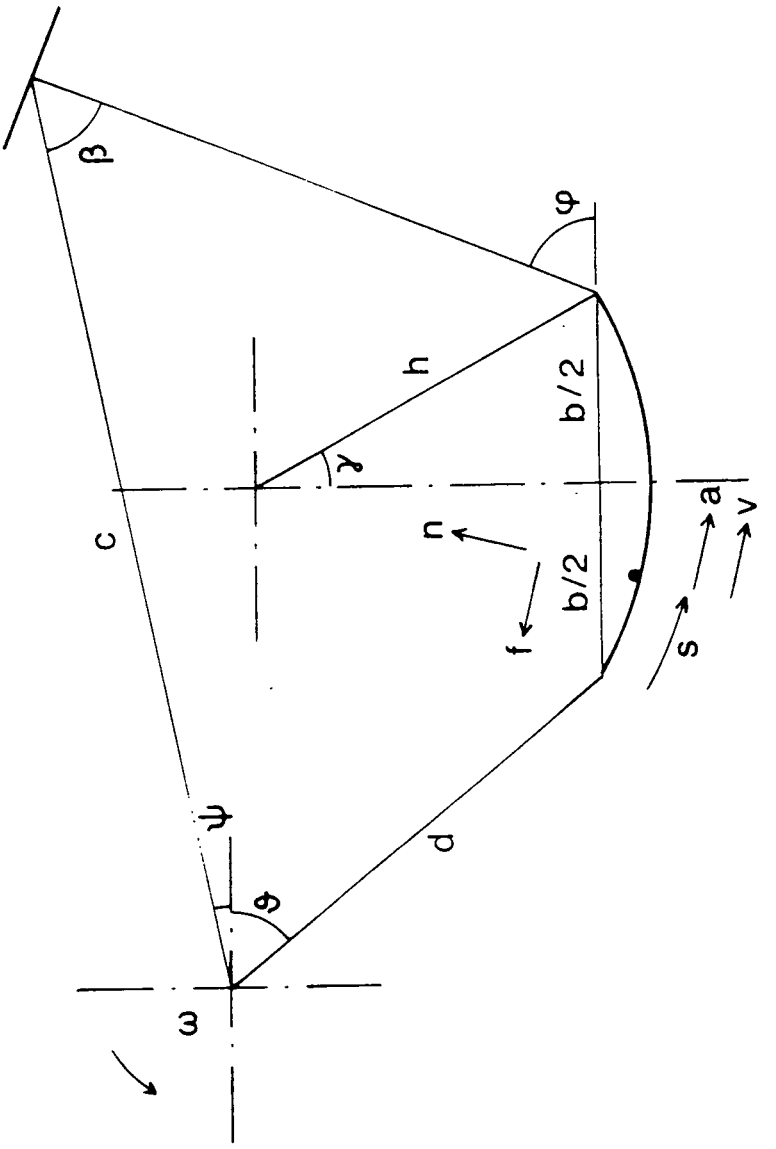

the upstream end of the wear part. The relative acceleration of the particle is obtained from equation (5).

The frictional and normal forces f and n are given by

$$f= (\omega^2(d \sin \theta+h(\cos\lambda -\cos\gamma))-a \sin\lambda +(v^2/h)\cos\lambda +2\omega v \cos\lambda)\sin\lambda$$
$$-(-\omega^2(d \cos \theta+b/2-h \sin\lambda)+a \cos\lambda +(v^2/h)\sin\lambda +2\omega v \sin\lambda)\cos\lambda \quad \ldots (17)$$

and

$$n= (-\omega^2(d \cos \theta+b/2-h \sin\lambda)+a \cos\lambda +(v^2/h)\sin\lambda +2\omega v \sin\lambda)\sin\lambda$$
$$+(\omega^2(d \sin \theta+h(\cos\lambda -\cos\gamma))-a \sin\lambda +(v^2/h)\cos\lambda +2\omega v \cos\lambda)\cos\lambda \quad \ldots (18)$$

For a large radius of curvature h, equations (16), (17) and (18) reduce, respectively, to equations (6), (2) and (3). For a convex surface, a negative value is specified for the radius of curvature.

By a similar method to that of Section 2.1.1 equation (19) may be derived for the impeller power P.

$$P=m\omega^2(b^2+2db \cos \theta)+m\omega v_0(d \sin \theta \cos\gamma +(d \cos \theta+b)\sin\gamma)-m\omega v_1 d \sin(\theta-\gamma) \quad \ldots (19)$$

The absolute exit velocity of the particle has components V_{xo} and V_{yo}, respectively tangential and normal to the wear part chord at the instant of exit. Thus, if v_o is the relative exit speed,

$$V_{xo} = v_o \cos\gamma +d\omega \sin \theta \quad \ldots (20)$$

and

$$V_{xo} = v_o \sin\gamma + \omega(b+d\cos\theta) \ldots (21)$$

The absolute exit speed and the anvil angle for normal impact are evaluated from equations (10), (11), (12), (13) and (14).

2.2 Computer Program

2.2.1 Impeller having flat wear parts

A FORTRAN computer program was developed, which models the performance of a Breakring having flat impeller wear parts. It calculates impeller power, absolute exit speed and anvil angle for normal impact over a range of equispaced values of particle - wear part coefficient of friction and wear part sweep angle. Output is in a form suitable for use by a contour generating program implementing subroutines from the GHOST-80 software library (Prior, 1985).

The input data comprises specification of the machine geometry and operating conditions, the range and number of values of coefficient of friction and wear part sweep, for which the performance is modelled, and the number of points along the wear part length, at which certain calculations are executed.

For each set of values of coefficient of friction and wear part sweep, equation (6) is integrated at equispaced points along the wear part length, to give relative speed. Integration is by the TEAPACK subroutine IVODE (Johnston, 1982), which uses the Runge Kutta Fehlberg method. If integration is successful at any point, then relative acceleration and normal and frictional forces are calculated, as detailed in Section

2.1.1. If integration is successful at the downstream end of the wear part, then the impeller power, the absolute exit speed and the anvil angle are calculated, also as detailed in Section 2.1.1. The performance data are stored as three two-dimensional arrays. The array dimensions correspond to coefficient of friction and wear part sweep. In general, for any value of coefficient of friction, the impeller operates only when the wear part sweep is less than some critical angle. If the wear part sweep exceeds this angle, then the particle stops or reverses. This is indicated by reduction of relative speed to zero or failure of the integration of equation (6). The values of coefficient of friction and wear part sweep at the limits of impeller operation are stored as a fourth two dimensional array.

The output data comprises the minimum and incremental values of coefficient of friction and wear part sweep, the numbers of values of coefficient of friction and wear part sweep, the performance data, the values of coefficient of friction and wear part sweep at the limits of impeller operation and the number of pairs of limiting values. If necessary, the distributions of relative speed and acceleration and normal and frictional forces along the wear part length, for each set of values of coefficient of friction and wear part sweep, may also be included in the output.

This program is listed in Appendix 1.

2.2.2 Impeller having cylindrical wear parts

The computer program described in Section 2.2.1 was adapted to model the performance of a Breakring having cylindrical impeller wear parts. The input data are as for the original program but includes the radius of curvature of the wear part.

Relative speed is evaluated by integration of equation (16), again by the TEAPACK subroutine IVODE. Relative acceleration, normal and frictional forces, impeller power, absolute exit speed and anvil angle are calculated as detailed in Section 2.1.2.

The output data are as for the original program.

2.2.3 Contour production

A FORTRAN computer program was developed, which, using the data generated by the programs of Sections 2.2.1 and 2.2.2, produces contours, against coefficient of friction and wear part sweep angle, of impeller power, absolute exit speed and anvil angle for normal impact. It implements subroutines from the GHOST-80 software library (Prior, 1985).

The input data comprises the minimum and incremental values of coefficient of friction and wear part sweep, the numbers of values of coefficient of friction and wear part sweep, the performance data, the values of coefficient of friction and wear part sweep at the limits of impeller operation and the number of pairs of limiting values.

Twenty equispaced contour values are calculated for impeller power, absolute exit speed and anvil angle. Contours are generated by the GHOST-80 subroutine CONTRA. Since CONTRA generates contours over a rectangular range, the region of the coefficient of friction-wear part sweep plane over which the impeller operates is divided into rectangular segments. The contours are pro-

duced for each segment individually.

The output is in the form of three plot descriptor files, which may be used with a graph plotting program to produce hard copies of the contours.

This program is listed in Appendix 2.

2.3 Results

As a preliminary investigation, the computer program of Section 2.2.1 was used to model the performance of the Breakring for a number of cases of particular interest. The results of one of these tests are plotted in Figure 5. They show the relative speed and acceleration of the feed material and the normal and frictional forces acting on a particle of units mass, as distributed along the wear part length. Also given are the absolute exit speed, the impeller power and the anvil angle required for normal impact.

The crusher dimensions were specified as for the prototype crusher (200 model) containing a six-port impeller. In determining the dimensions for the impeller, it was assumed that the initial contact between the feed material and wear part occurs at the upstream tip. Typical values were specified for the impeller speed and mass flowrate. The coefficient of friction between the feed material and the wear part surface was set at 0.1 (Garland, 1983). The relative speed of the feed material at the upstream end of the wear part was set at 0.1 m/s. Although the exact relative speed was unknown, it was thought to be small due to the effect of the breakring. Furthermore, results of later tests showed that this quantity had little effect on conditions downstream.

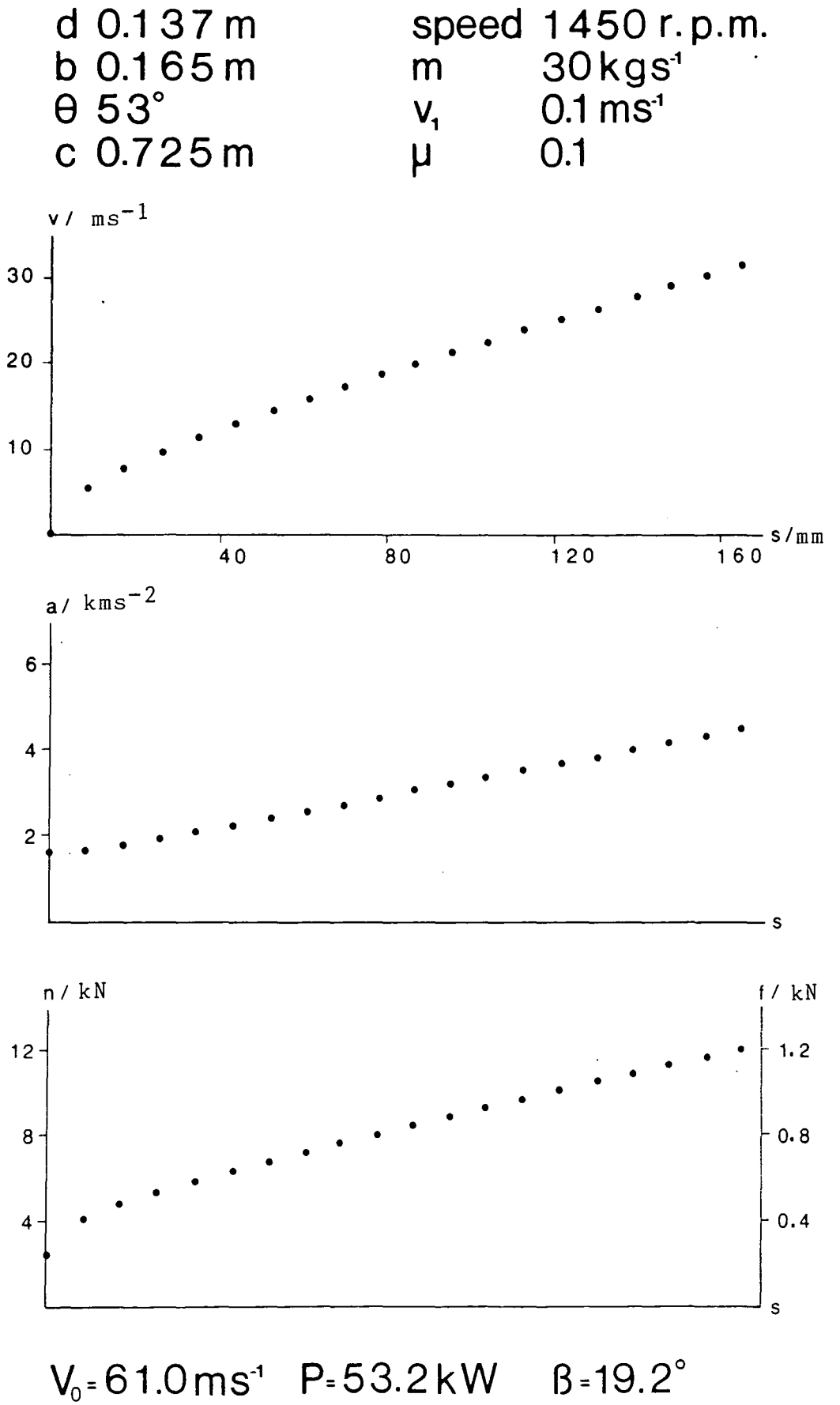

Figure 5

Performance of Breakring: 200 Model, Six-Port Impeller

Conditions were evaluated at twenty equispaced positions including the two ends of the wear part. The four quantities plotted in Figure 5 increase monotonically with distance from the upstream end of the wear part. The effect of a change in the relative speed of the feed material at the upstream end of the wear part was examined. For an upstream relative speed of 1.0 m/s, it was seen that conditions converged to those of the previous case within 5mm from the upstream point. Even for an upstream relative speed of 10 m/s, the downstream relative speed was only 1.2 m/s greater than that for an upstream speed of 0.1 m/s. The reason for this stabilisation of conditions is that, if the upstream relative speed is increased, then the normal and frictional forces increase also. The acceleration reduces and the relative speed tends to the value for low upstream relative speed.

Further tests revealed that, for all values of coefficient of friction between the feed material and the wear part surface, only very small negative values of wear part sweep angle can be tolerated. For larger negative values of wear part sweep angle, the normal force reduces to zero at the upstream end of the wear part and, as may be shown graphically or otherwise, the feed material separates from the wear part surface and remains detached or reattaches at some point further downstream. Such behaviour is undesirable. These impeller configurations are of little interest to the designer.

It was shown also that, for large positive wear part sweep angle and/or large coefficient of friction, the feed material tends to stop in the impeller. Under such conditions, the normal and frictional forces are large and tend rapidly to decelerate the particle. Thus, un-

less the upstream speed is sufficiently high, the particle slows to a standstill. If the coefficient of friction is very low, flow can be maintained with a wear part sweep angle of 90° provided the upstream speed is greater than zero. At higher values of coefficient of friction, the maximum permissible wear part sweep angle is correspondingly lower. For the present six port impeller configuration, the highest value of coefficient of friction which can be tolerated is 0.742, when the upstream relative speed of the feed material is 0.1 m/s. The material flow could of course, be maintained with higher values of coefficient of friction and wear part sweep angle, if the upstream relative speed were sufficiently great. These limits to machine operation are not encountered in practice and are of purely academic interest.

Following the modelling of Breakring performance for various individual values of coefficient of friction and wear part sweep angle, the computer programs of Sections 2.2.1, 2.2.2 and 2.2.3 were used to produce contours of impeller power, absolute exit speed and anvil angle for normal impact over a range of values of friction coefficient and wear part sweep angle. The machine dimensions and operating conditions were again specified as for standard crushing operation by a Breakring containing a six-port impeller. The upstream particle speed was set at 0.1 m/s.

Figures 6, 7 and 8 show contours of absolute exit speed.

Figure 6 refers to an impeller having flat side wear parts. It is seen that the absolute exit speed decreases with increasing coefficient of friction. It is seen also that the maximum exit speed is generally attained if the wear part sweep angle is between 15° and 35°, depending on the coefficient of friction. Although

Figure 6

Contours of Absolute Exit Speed: Flat Impeller Wear Parts

Contour Number	Speed (m/s)
1	48
2	49
3	50
4	51
5	52
6	53
7	54
8	55
9	56
10	57
11	58
12	59
13	60
14	61
15	62
16	63
17	64

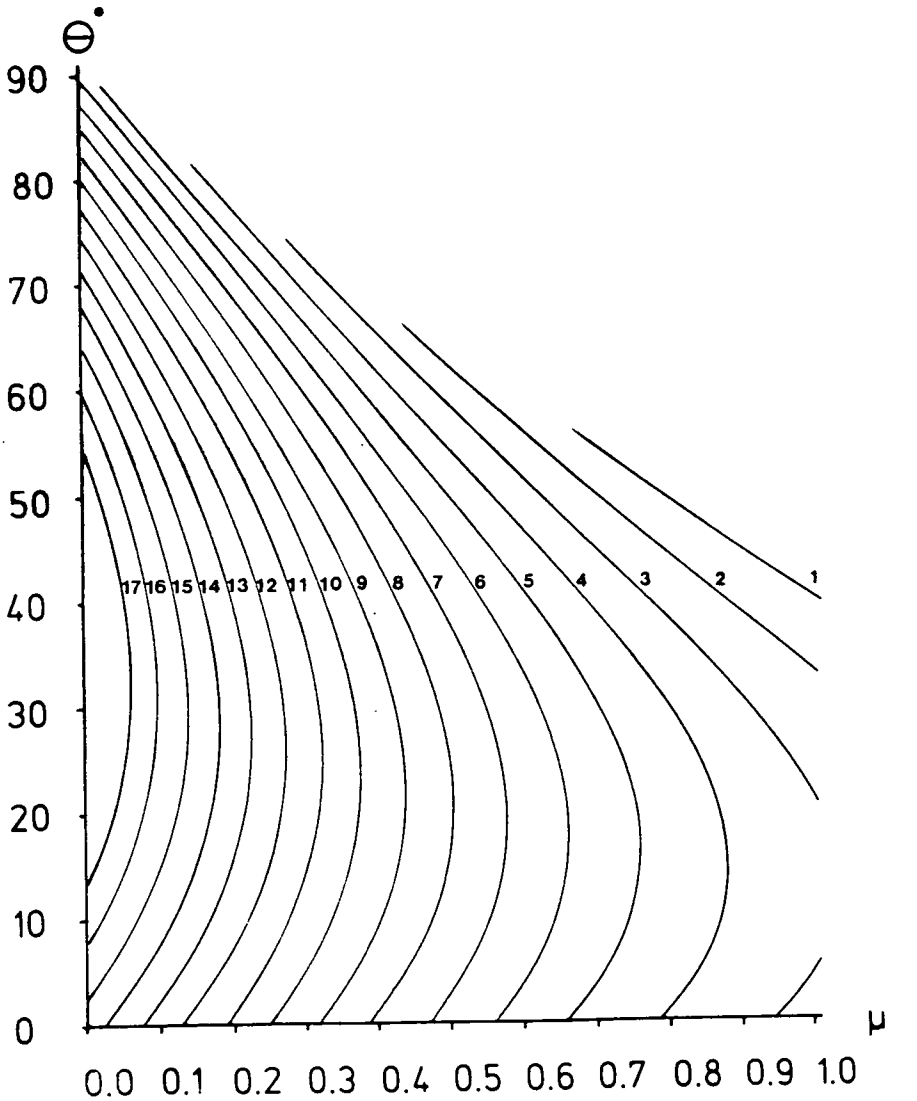

the relative exit speed is always highest when the wear part surface is radial or slightly back swept, the absolute exit speed is greater when the relative exit velocity and wear part tip velocity are nearer parallel. (It can, in fact, be shown that the relative exit velocity and wear part tip velocity are parallel for a wear part sweep angle of approximately 180°.)

The envelope defining the limits of impeller operation gives the wear part sweep angle at 90° for zero coefficient of friction and decreasing with increasing coefficient of friction.

In the contours of Figure 7, which refer to an impeller having concave cylindrical wear parts, the impeller operation is defined for wear part sweep angles ranging from approximately 25° to approximately 115° at zero coefficient of friction. At these limits, the tangent to the upstream end of each wear part is inclined at respectively zero and 90° to the radius from the centre of rotation.

The maximum exit speed is attained when the wear part sweep angle is approximately 25°.

In the contours of Figure 8, which refer to an impeller having convex cylindrical wear parts, the impeller operation is defined for wear part sweep angles ranging from approximately -25° to approximately 65° at zero coefficient of friction. At these limits, the tangent to the upstream end of each wear part is once more inclined at respectively zero and 90° to the radius from the centre of rotation.

The maximum exit speed is attained when the wear part sweep angle is between 25° and 45°.

Figure 7

Contours of Absolute Exit Speed: Concave Impeller Wear Parts

Contour Number	Speed (m/s)
1	36.9
2	39.0
3	41.1
4	43.3
5	45.4
6	47.5
7	49.6
8	51.8
9	53.9
10	56.0
11	58.2
12	60.3
13	62.4
14	64.5
15	66.7
16	68.8
17	70.9
18	73.1

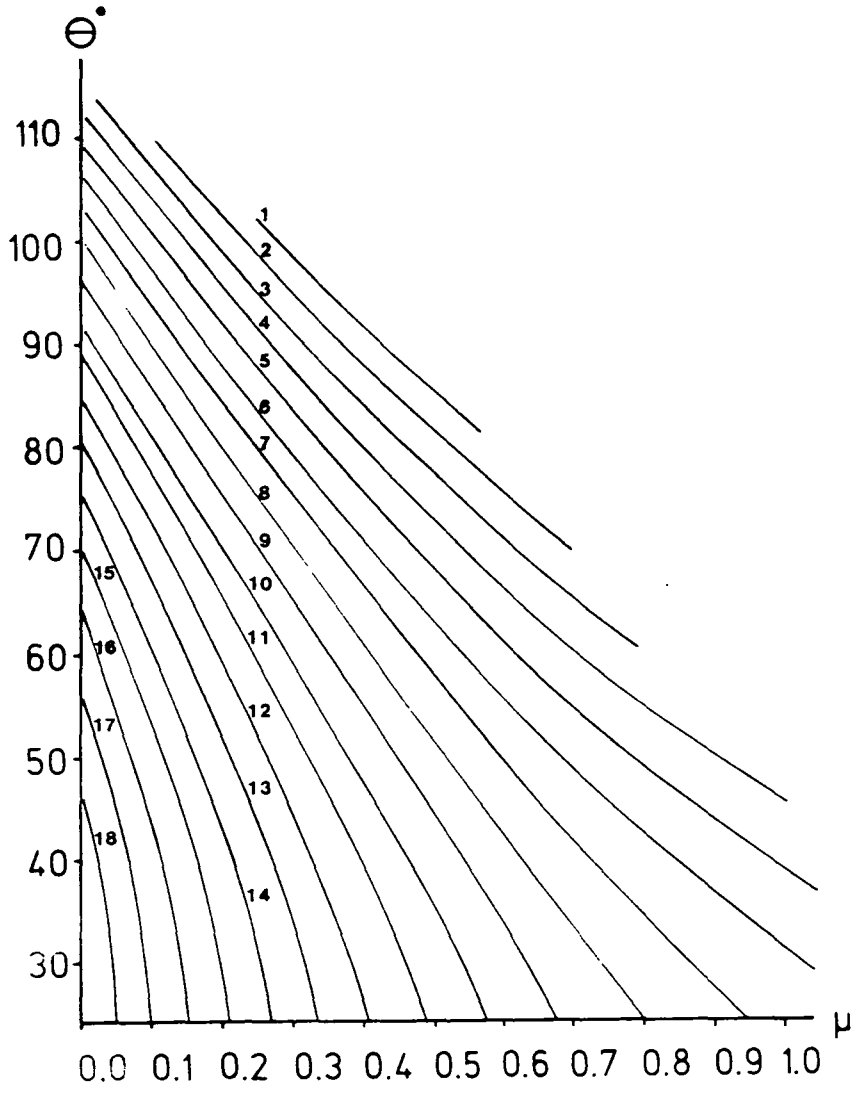

Figure 8

Contours of Absolute Exit Speed: Convex Impeller Wear Parts

Contour Number	Speed (m/s)
1	37.8
2	38.7
3	39.6
4	40.6
5	41.5
6	42.4
7	43.3
8	44.2
9	45.1
10	46.0
11	46.9
12	47.8
13	48.8
14	49.7
15	50.6
16	51.5
17	52.4
18	53.3

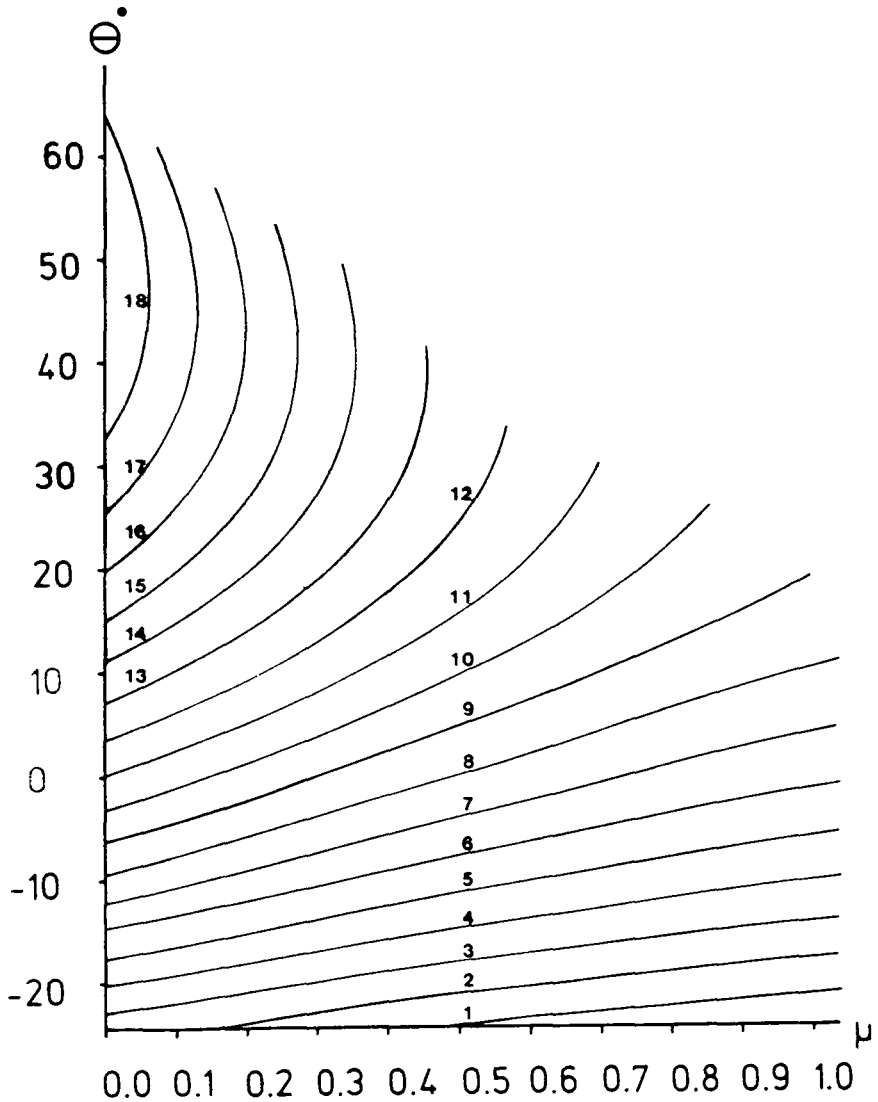

Figures 9, 10 and 11 show contours of impeller power. Equation (22) gives the standard expression for impeller power, familiar from the theory of turbomachinery.

$$P = m\omega(e\ V_{co} - dV_{ci})...(22)$$

P, m, ω and d are as defined in Section 2.1.e, V_{co} and V_{ci} represent, respectively, the radius of the downstream end of the wear part and the circumferential components of absolute material velocity at the downstream and upstream ends of the wear part. Since the radii of the two ends of the wear part are approximately constant and the upstream absolute speed is low, the impeller power is dependent primarily on the magnitude of the circumferential component of the absolute exit velocity, which, for flat and concave cylindrical wear parts, is approximately equal to the absolute exit speed. Thus, the contours of Figures 9 and 10, which refer to impellers having respectively flat and concave cylindrical wear parts, are similar to those of, also respectively, Figures 6 and 7.

Figure 11 refers to an impeller having convex cylindrical wear parts. For such an impeller, the circumferential component of the relative exit velocity is generally opposed in direction to the wear part tip velocity. Thus the circumferential component of the absolute exit velocity has the greatest magnitude when the relative exit speed is low. This condition is satisfied when the coefficient of friction and wear part sweep angle are high. Thus the impeller power is greatest for high coefficient of friction and wear part sweep angle.

Figures 12, 13 and 14 show contours of anvil angle for normal impact. For flat, concave and convex wear parts, this angle is a complex function of the crusher geometry and operating conditions. In general, it has the lowest

Figure 9

Contours of Impeller Power: Flat Impeller Wear Parts .

Contour Number	Power (kW)
1	36.0
2	37.5
3	39.0
4	40.5
5	42.0
6	43.5
7	45.0
8	46.5
9	48.0
10	49.5
11	51.0
12	52.5
13	54.0
14	55.5
15	57.0

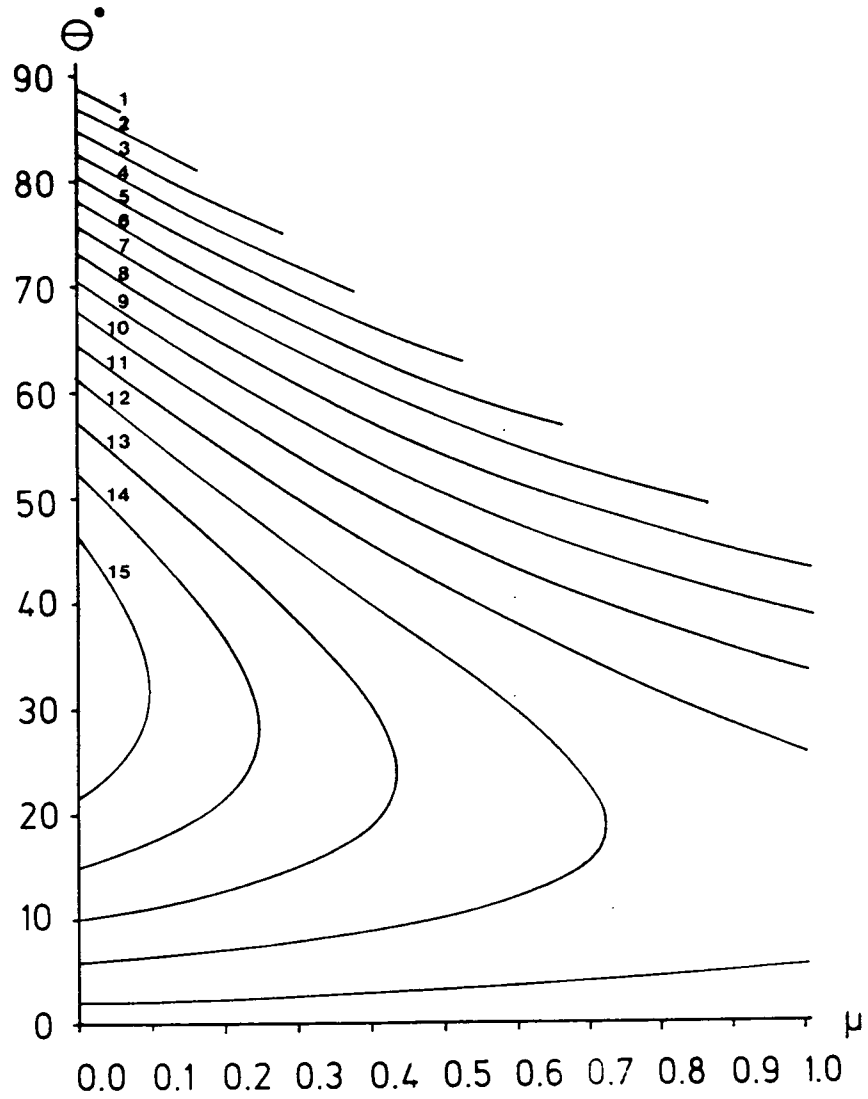

Figure 10

Contours of Impeller Power: Concave Impeller Wear Parts

Contour Number	Power (kW)
1	19.5
2	23.0
3	26.5
4	30.0
5	33.5
6	37.0
7	40.5
8	44.0
9	47.5
10	51.0
11	54.5
12	58.0
13	61.5
14	65.0
15	68.5
16	72.0
17	75.5

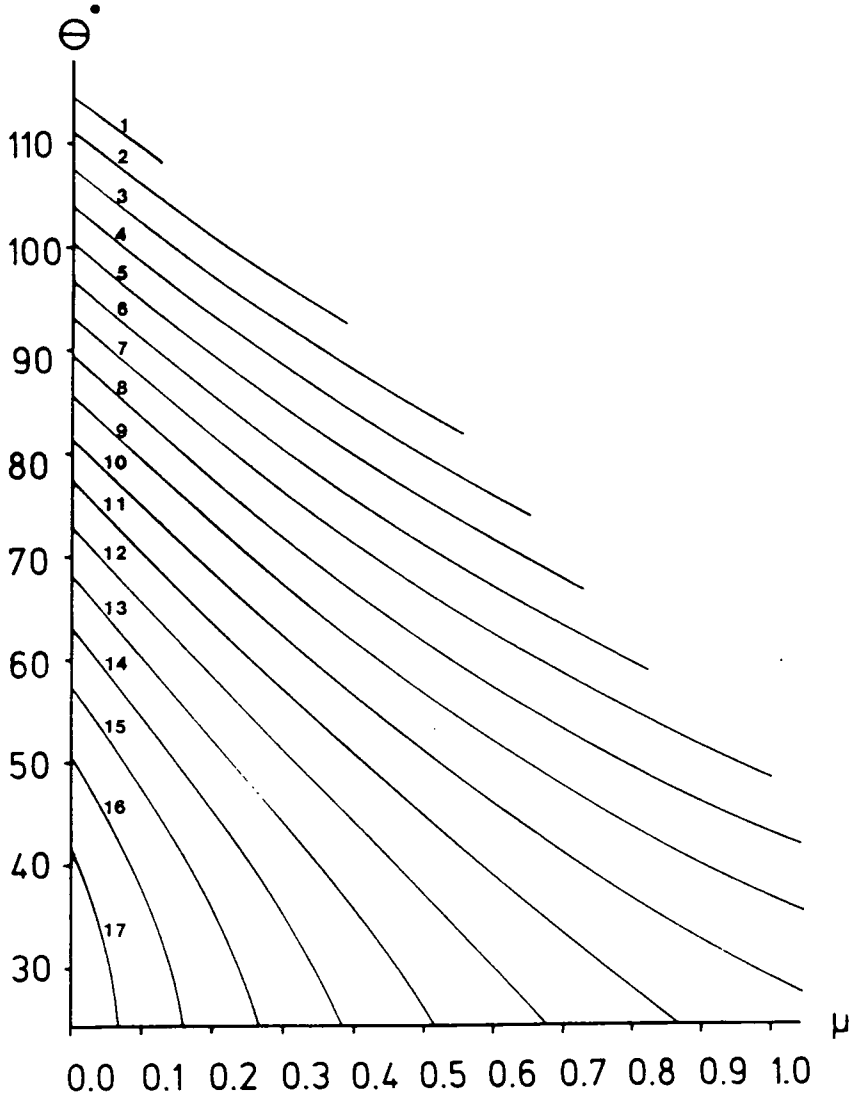

Figure 11

Contours of Impeller Power: Convex Impeller Wear Parts

Contour Number	Power (kW)
1	17.6
2	18.8
3	20.0
4	21.3
5	22.5
6	23.7
7	24.9
8	26.1
9	27.4
10	28.6
11	29.8
12	31.0
13	32.2
14	33.5
15	34.7
16	35.9
17	37.1
18	38.3

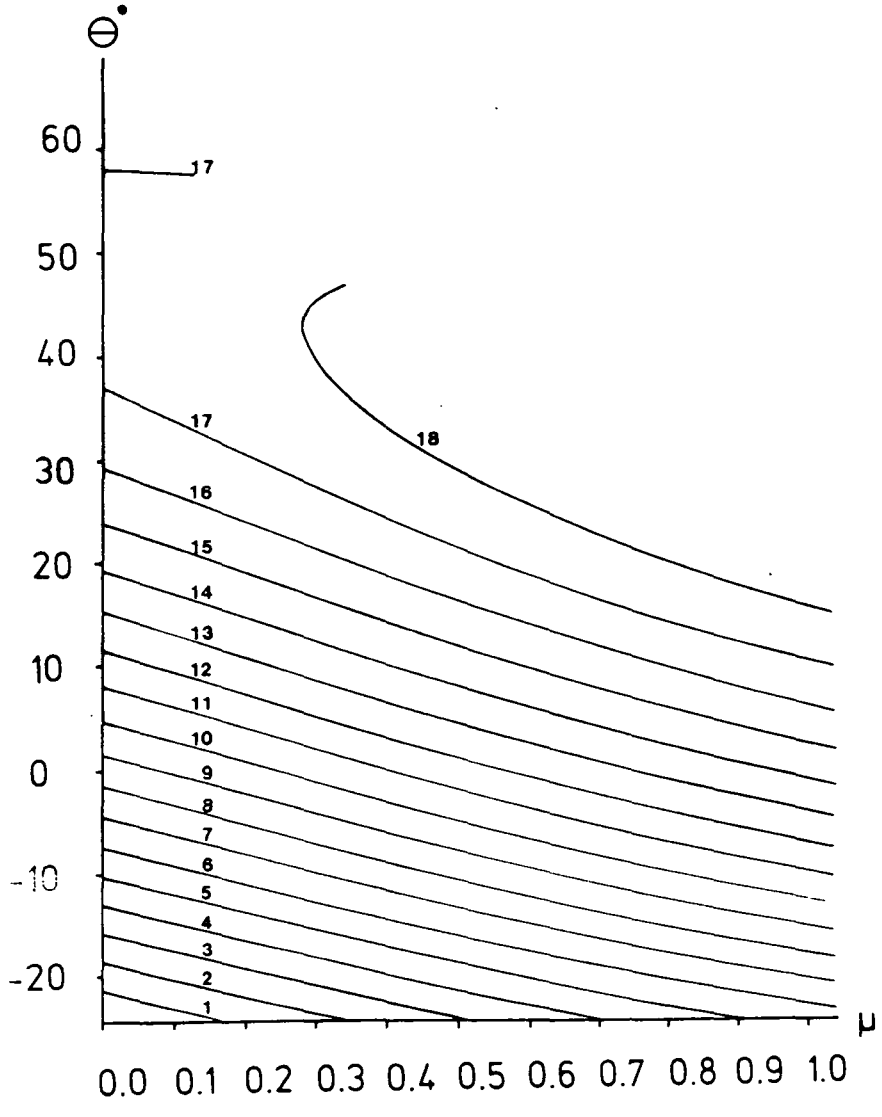

Figure 12

Contours of Anvil Angle: Flat Impeller Wear Parts

Contour Number	Angle (Degrees)
1	16.4
2	16.7
3	17.1
4	17.5
5	17.8
6	18.2
7	18.6
8	18.9
9	19.3
10	19.7
11	20.0
12	20.4
13	20.8
14	21.2
15	21.5
16	21.9
17	22.3
18	22.6

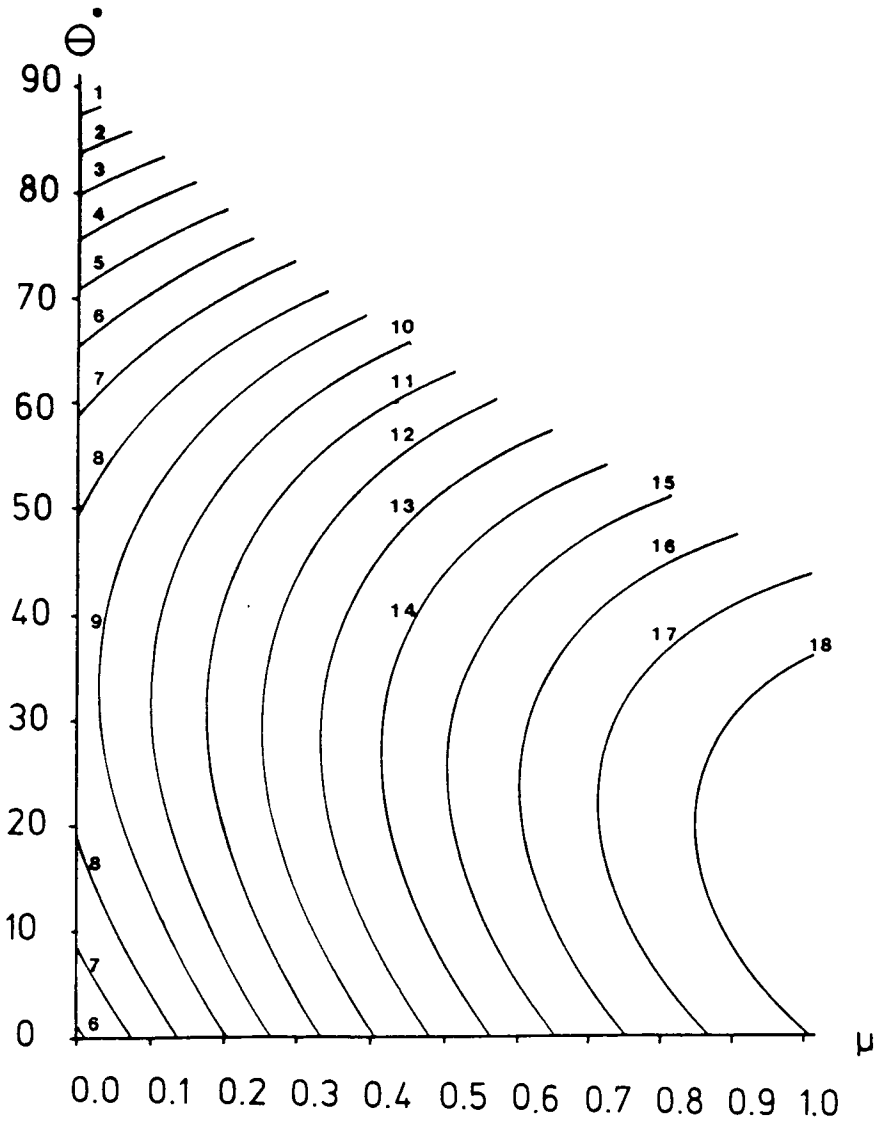

Figure 13

Contours of Anvil Angle: Concave Impeller Wear Parts .

Contour Number	Angle (Degrees)
1	14.7
2	15.2
3	15.8
4	16.3
5	16.9
6	17.4
7	18.0
8	18.5
9	19.1
10	19.7
11	20.2
12	20.8
13	21.3
14	21.9
15	22.4
16	23.0
17	23.5

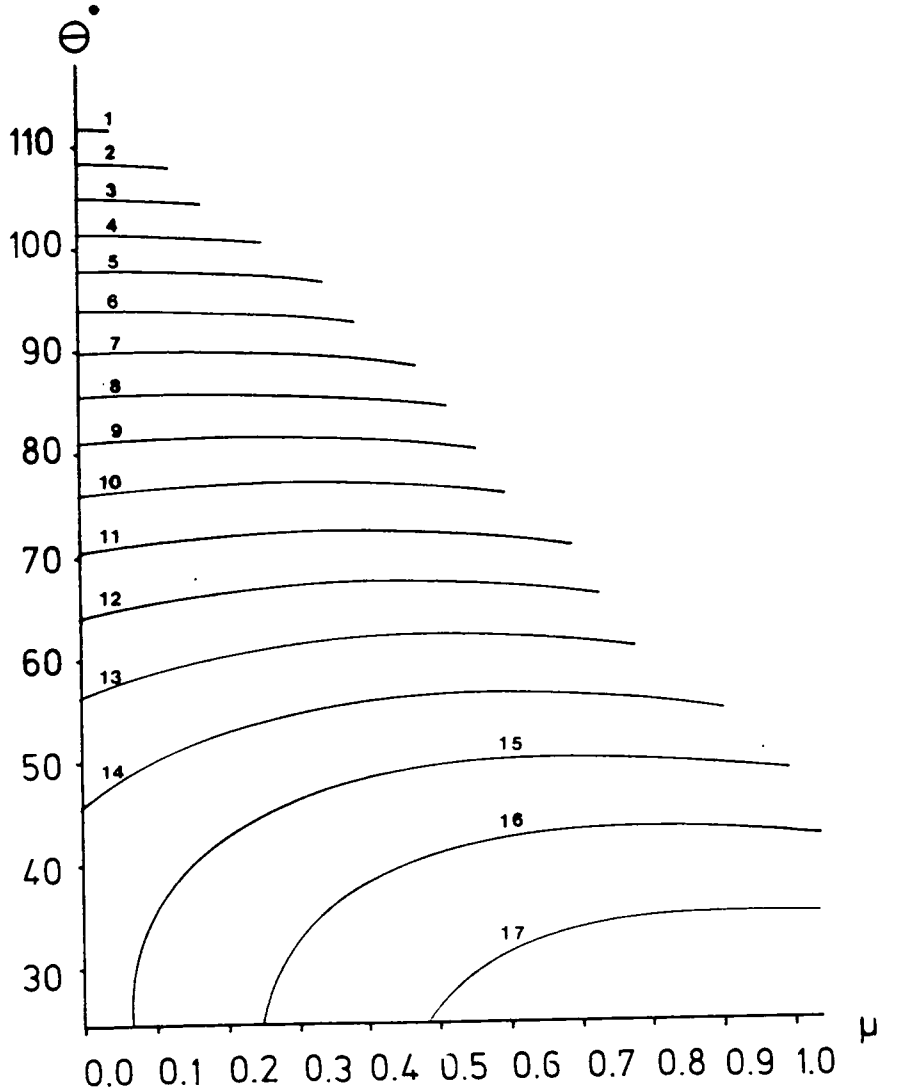

Figure 14

Contours of Anvil Angle: Convex Impeller Wear Parts

Contour Number	Angle (Degrees)
1	14.1
2	14.5
3	14.8
4	15.2
5	15.6
6	15.9
7	16.3
8	16.7
9	17.0
10	17.4
11	17.8
12	18.1
13	18.5
14	18.9
15	19.2
16	19.6
17	19.9
18	20.3

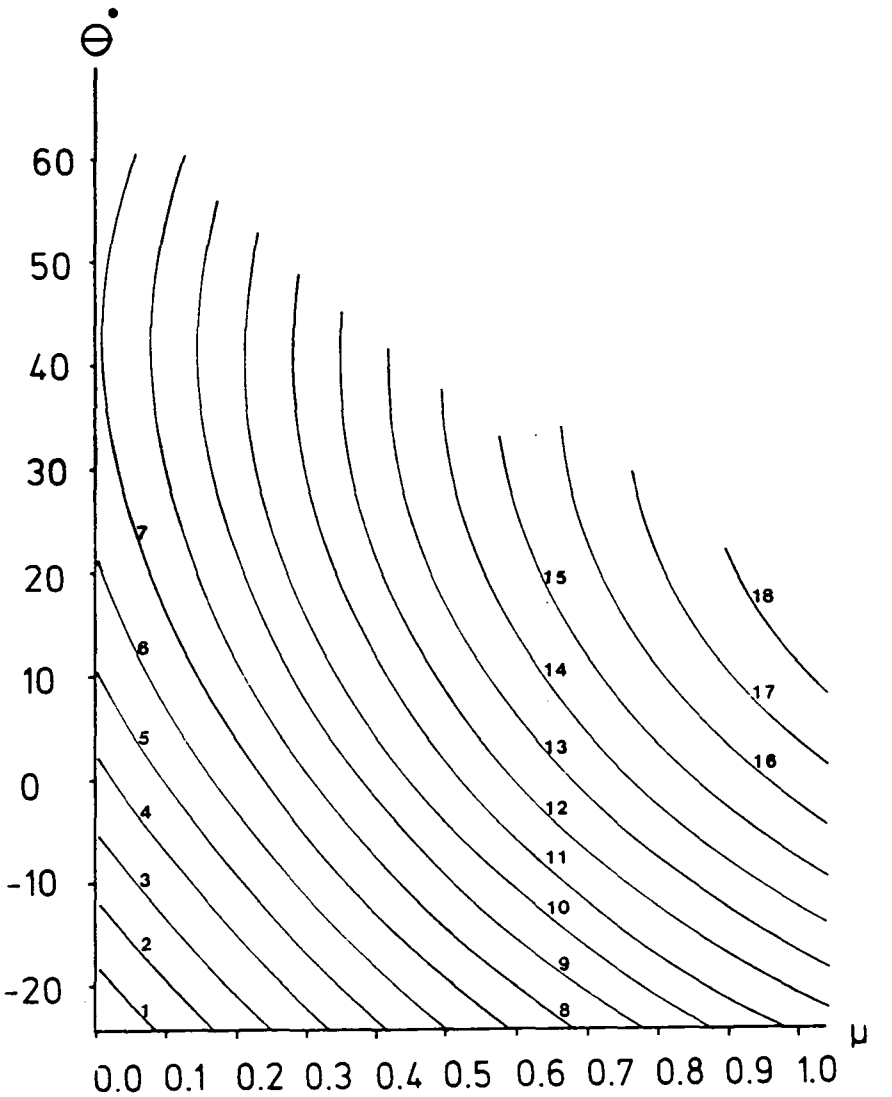

value for smallest coefficients of friction.

3. COMPUTATION OF THE FLOW OF MATERIAL IN THE BREAKRING IMPELLER

3.1 Analysis

The action of a single particle in the Breakring impeller is analysed. The analysis is valid for any specified wear part profile. Since the motion of material within the impeller is approximately horizontal, a two-dimensional model is considered. The following refers to the arrangement shown in Figure 15. The particle is treated as a unit mass subjected only to inertia and frictional and normal forces, f and n, at the wear part surface. The frictional and normal forces are related by equation (1). The impeller rotates anticlockwise at angular speed ω. The particle makes contact with an impeller wear part at some point 1 and, in general, slides some distance along the wear part towards the exit port. The wear part downstream of point 1 is approximated by a series of straight segments. The endpoints of each segment are specified with respect to horizontal orthogonal axes xy rotating with the impeller and originating at the centre of the rotation. At point 1, the particle has speed v_1, relative and parallel to the first segment. v_1 is low and directed downstream. The normal force acting on the particle at the midpoint of the i^{th} segment is given by

$$n_i=\omega^2 R_i \sin \alpha_i+2\omega v_i+(v_i^2/\delta s_i) \sin (\beta_{i+1} -\beta_i) \quad ...(23)$$

where R is the radius from the centre of rotation to the segment midpoint, α is the angle between the segment tangent and the radius R, v is the relative speed of the particle, δs is the segment length and β is the angle between the segment tangent and the x-axis. The first

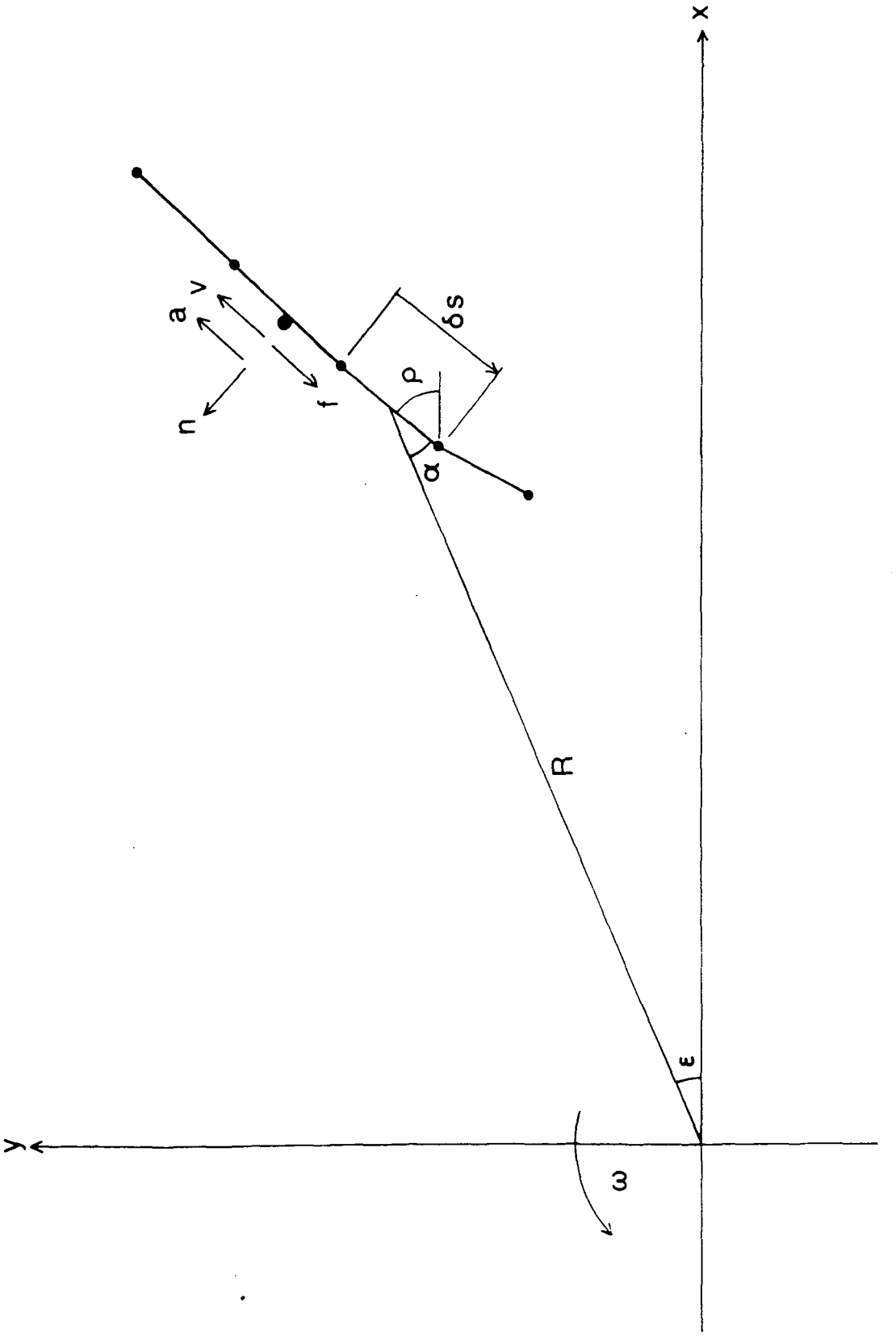

Figure 15

Breakring Impeller Two-Dimensional Arrangement

term on the right hand side of equation (23) gives the normal component of centrifugal force (Higginson, 1974). The second term gives the Coriolis force (Higginson, 1974). The third term gives the normal force required to turn the particle through the angle ($\beta_{i+1} - \beta_i$) between adjacent segments. This term is accurate if the velocities on adjacent segments are similar. This condition is satisfied if the segments are short.

If the normal force is greater than zero, then at the midpoint of the i^{th} segment,

$$a_i = \omega^2 R_i - f \quad \ldots (24)$$

where a is the relative acceleration of the particle. At the upstream endpoint of the $(i+1)^{th}$ segment,

$$v_{i+1} = (v_i^2 + 2a_i s_i)^{1/2} \quad \ldots (25)$$

If the relative speed of the particle reduces to zero, impeller operation is considered to have failed.

If the normal force reduces to zero, the particle separates and follows a trajectory of constant velocity until again constrained by the wear part. If the particle separates from the i^{th} segment, then it has absolute velocity components V_{ix} and V_{iy} parallel to the X and Y axes. The X and Y axes are fixed axes coincident with the x and y axes at the instant of separation.

V_{ix} and V_{iy} are given by

$$V_{ix} = v_i \cos\beta_i - \omega y_i \quad \ldots (26)$$

$$V_{iy} = v_i \sin\beta_i + \omega x_i \quad \ldots (27)$$

For the particle to reattach to the surface of the k^{th}

segment

$$\sigma = \epsilon_k \ldots (28)$$

when

$$Q = R_k \ldots (29)$$

Q is the radius from the centre of rotation of the particle position, σ the angle between the radius Q and the x-axis and ϵ the angle between the radius R and the x-axis.

It may be shown that, when $Q = R_k$

$$T=x_i V_{ix}+y_i V_{iy}+((x_i V_{ix}+y_i V_{iy})^2-(V_{ix}^2+V_{iy}^2)(x_i^2+y_i^2-R_k^2))^{1/2}$$

$$\ldots (30)$$

and

$$\Sigma = \arctan ((y_i+V_{iy}T)/(x_i+V_{ix}T)) \ldots (31)$$

where T is the time elapsed since separation and Σ is the angle between the radius Q and the X-axis. It is apparent that

$$\sigma=\Sigma -\omega T \ldots (32)$$

Thus equation (28), the condition for reattachment, becomes

$$\arctan ((y_i+V_{iy}T)/(x_i+V_{ix}T))-\omega T = \epsilon_k \ldots (33)$$

x_i, y_i and ϵ_k are obtained from the wear part profile. V_{ix}, V_{iy} and T are obtained from equations (26), (27) and (30) respectively.

If the particle reattaches on the k^{th} segment, the reattachment speed v_k and reattachment angle χ are given by

$$v_k = ((V_{iy} - X_k)^2 + (V_{ix} + Y_k)^2)^{1/2} \quad \ldots (34)$$

and

$$\chi = \beta_k + \omega T - \arctan ((V_{iy} - X_k)/(V_{ix} + Y_k)) \quad \ldots (35)$$

The reattachment speed is the relative speed, at reattachment, between the particle and the segment mid-point at which reattachment occurs. The reattachment angle is the angle, at reattachment, between the tangent to the segment at which reattachment occurs and the direction of the relative velocity of the particle.

If the reattachment angle is less than zero, then the particle skims the surface and separates again immediately. The velocity of the particle is assumed to be unchanged by this contact.

If the reattachment angle is greater than or equal to zero, then the particle reattaches to the surface and

$$v_{k+1} = v_k \cos \chi \ldots (36)$$

3.2 Computer program

A computer program was developed, which models the action of a single particle of unit mass on an impeller wear part of specified, segmentised profile. It calculates the normal and frictional forces acting on the particle and the relative speed and acceleration of the particle, as distributed along wear part. If, at any position, the normal force is found to reduce to zero,

so that the particle separates from the wear part surface, the program calculates the position at which reattachment occurs as well as the reattachment speed and the reattachment angle.

The input data comprises the number of segment endpoints, the xy coordinates of the endpoints, the angular speed of the impeller, the coefficient of friction between the particle and the wear part and the upstream relative speed of the particle.

The program calculates, for consecutive segments, the normal and frictional forces and the relative acceleration at the midpoint and the relative speed at the downstream endpoint, as detailed in Section 3.1. If the normal force is positive, this procedure is repeated for the next segment and so on up to the last segment. If the normal force is found to reduce to zero, indicating separation of the particle, then a subroutine is called, which checks for reattachment at consecutive midpoints downstream of that at which separation occured, again as detailed in Section 3.1. When the reattachment position has been located, the subroutine calculates the reattachment speed and reattachment angle and the relative speed at the endpoint downstream of the reattachment point, also as detailed in Section 3.1. The program then returns to the main routine.

The output data comprises, for all segments, the midpoint and endpoint xy coordinates and, for segments at which the particle is attached, the upstream relative speed and the midpoint relative acceleration and normal and frictional forces, together with, where applicable, the reattachment speed and angle.

This program is listed in Appendix 3.

3.3 Results

Six cases of particular interest were modelled with the computer program of Section 3.2. The results of these tests are plotted in Figures 16-19, 21 and 22. Each set of results shows the wear part profile, the distributions of relative speed and acceleration and frictional and normal forces along the wear part length and, when separation is indicated, the reattachment speed and reattachment angle.

In all tests, the wear part profile was taken from a 165 mm tile mounted in a six-port impeller. It was assumed that the feed material meets the upstream end of the wear part. The standard value of 1450 r.p.m. was specified for the impeller speed. The relative speed of the feed particle at the upstream end of the wear part was set at 0.1 m/s. In all tests, the wear part profile endpoints were equispaced at 1 mm intervals in the x-direction. Because of the closeness of the points, they were joined, in Figures 16-19, 21 and 22 to form continuous curves.

The first test modelled the same case as that shown in Figure 5 and was intended as a check on the accuracy of the program of Section 3.2. The wear part profile was approximated by a straight line. The coefficient of friction between the particle and the wear part was set at 0.1 (Garland, 1983). The results are shown in Figure 16 and agree well with those of Figure 5. The slight decrease in relative acceleration over the first two millimeters is a consequence of the initial build up of the relative speed and normal and friction forces.

The second test modelled the effect of a shallow depression in the upstream region of the wear part. Such a depression develops in practice and results from the ac-

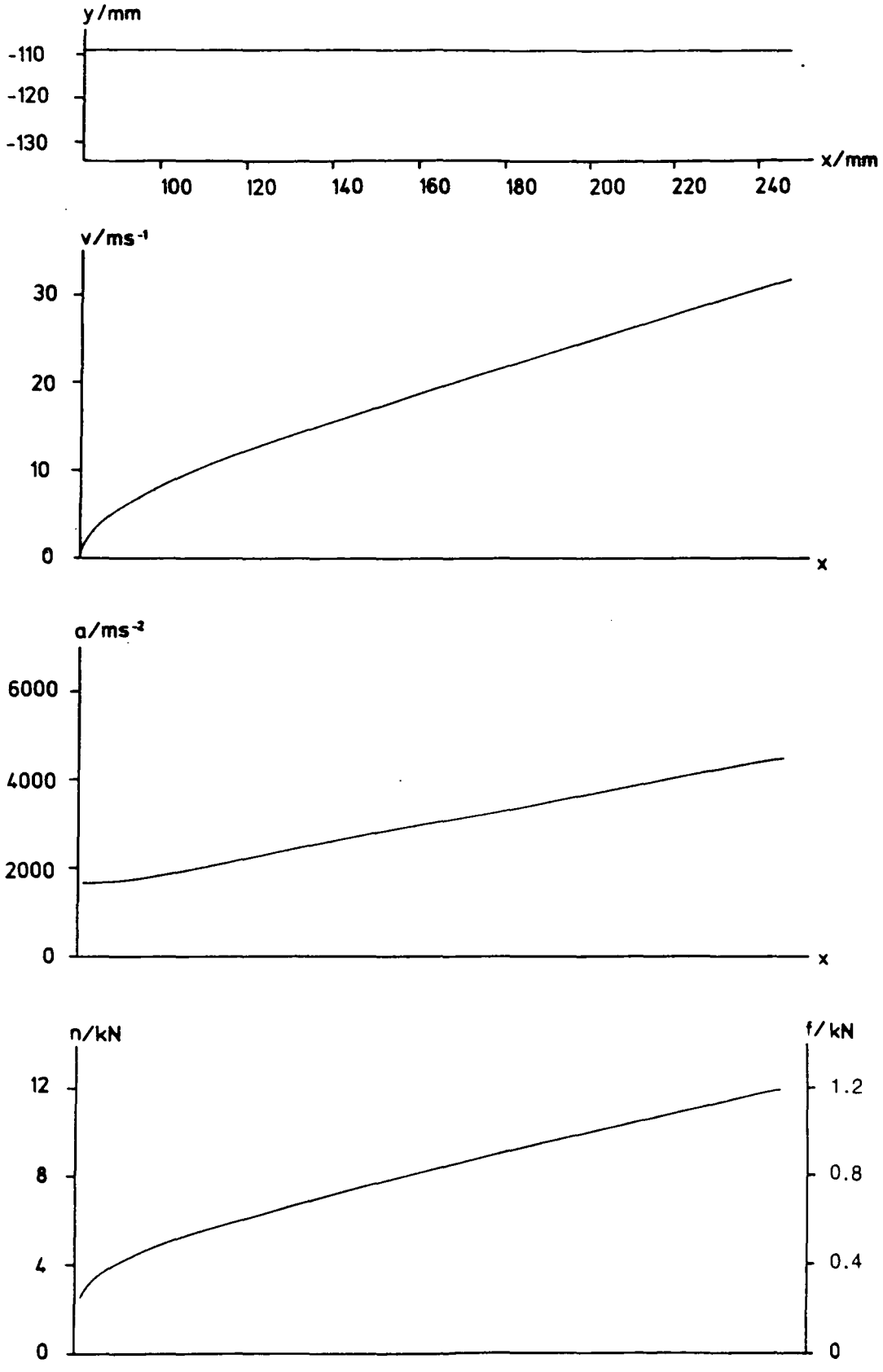

Figure 16

Action of Material in Breakring Impeller: Profile 1

tion of feed material entering the port and being accelerated rapidly to impeller speed ωR. The depression of length 115mm and depth 2 mm was approximated by half a wavelength of a sine curve. In this and the following three tests, the feed material - wear part coefficient of friction was set at 0.05 (Garland, 1983). The results of this test are shown in Figure 17. The particle is seen to separate from the downstream end of the depression and reattach a short distance downstream.

In the third test, the depth of the depression was increased to 8 mm. The results are shown in Figure 18. The increase in the depth of the depression has a significant effect on the trajectory of the particle, which leaves the downstream end of the depression at a steeper angle and consequently reattaches further downstream, with an increased reattachment speed and reattachment angle. It is believed that the impact of reattachment is responsible for the formation of the second, downstream depression, observed on the worn wear parts of both six-port and two-port impellers.

The fourth test modelled the effect of a further increase in the depth of the upstream depression to 10 mm and the introduction of a downstream depression of length 50 mm and depth 8 mm, which also was approximated by half a wavelength of a sine curve. The results, which are shown in Figure 19, indicate that reattachment is displaced further downstream and that the reattachment speed is further increased.

Figure 20 illustrates the relative trajectories of the detached particles in the second and third tests. The horizontal axis represents the unworn surface of the wear part. The axes intersect at the downstream end of the upstream depression i.e. the point at which separation occurs. Curve C represents part of a depression of

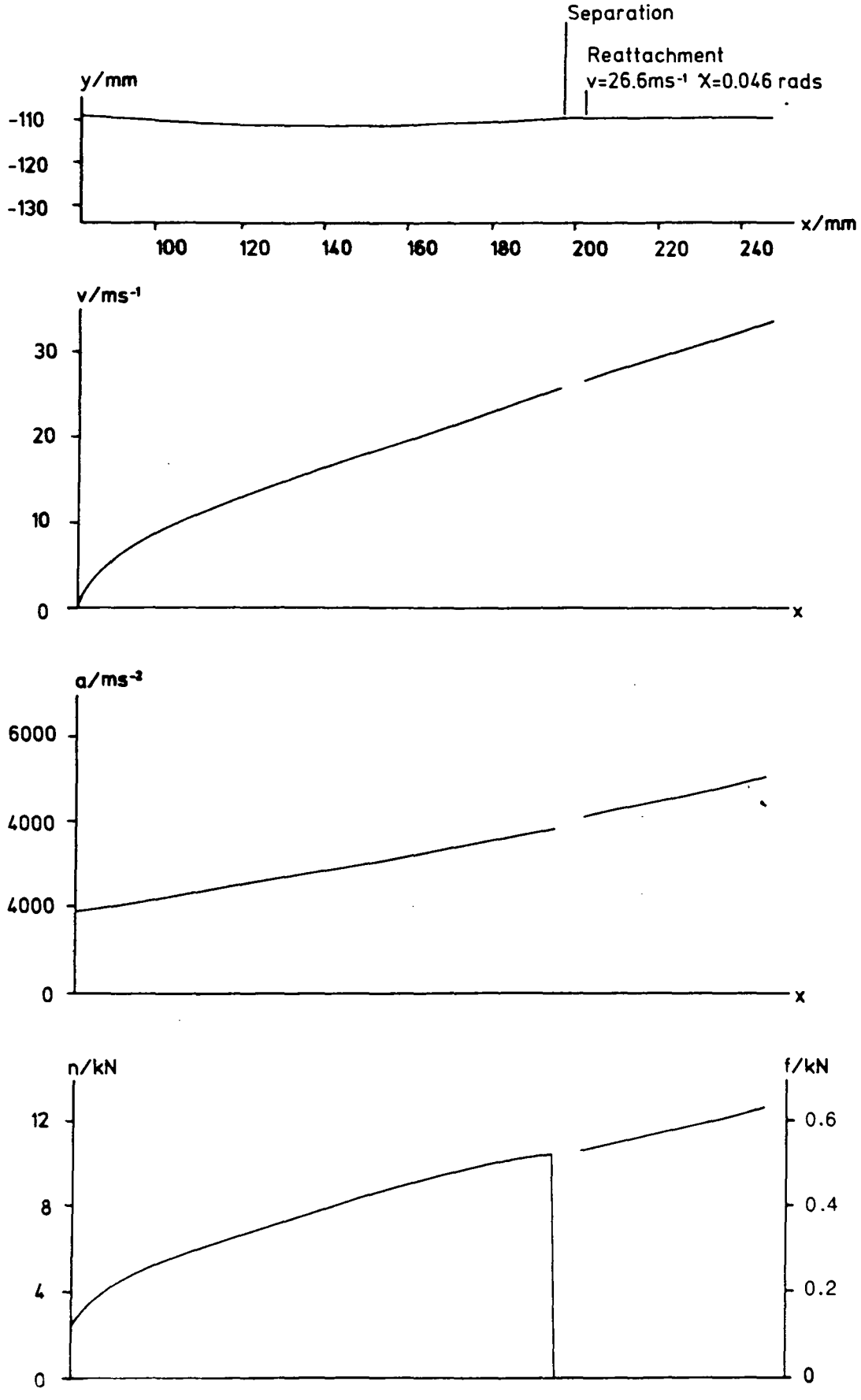

Figure 17

Action of Material in Breakring Impeller: Profile 2

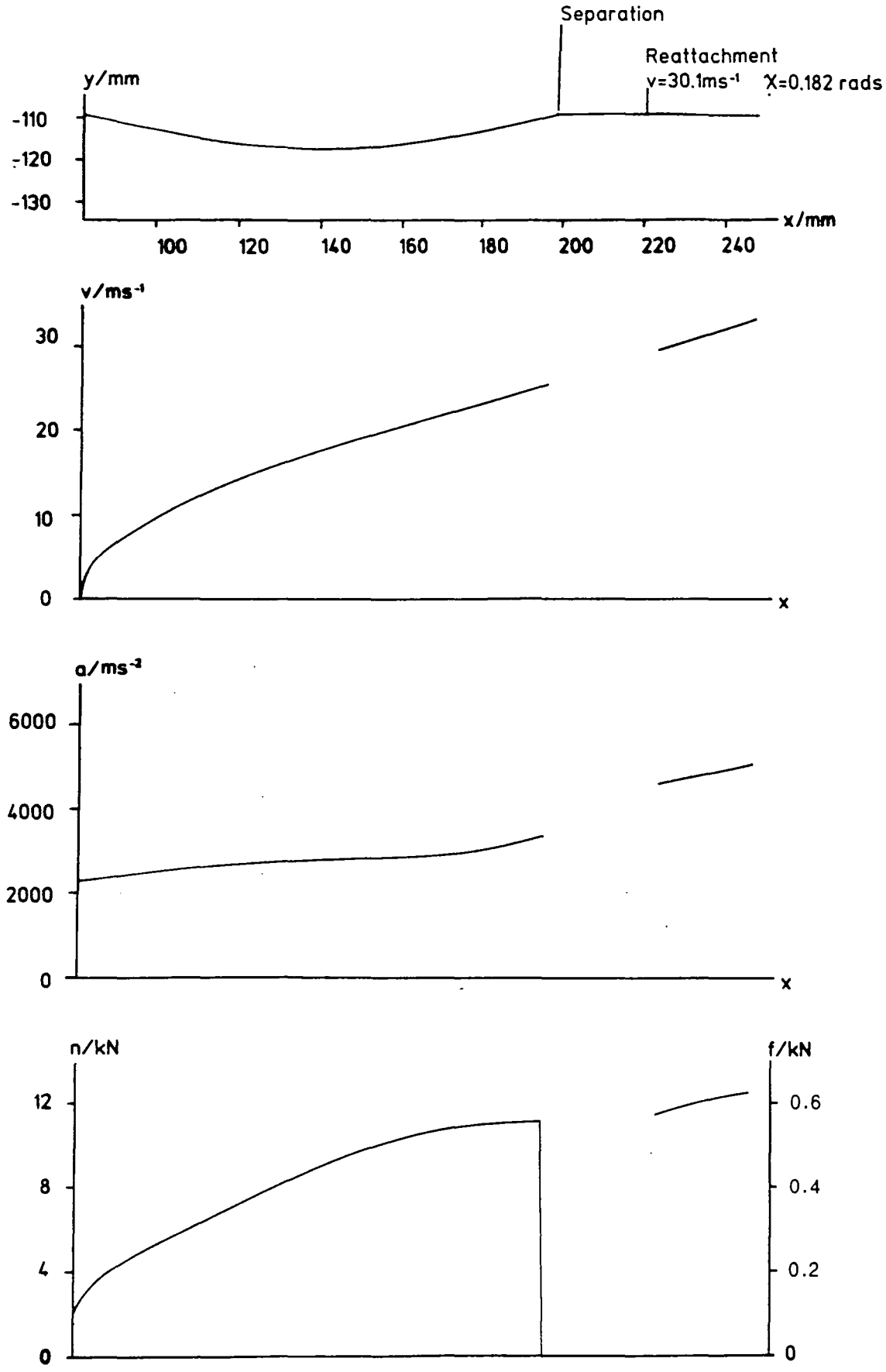

Figure 18

Action of Material in Breakring Impeller: Profile 3

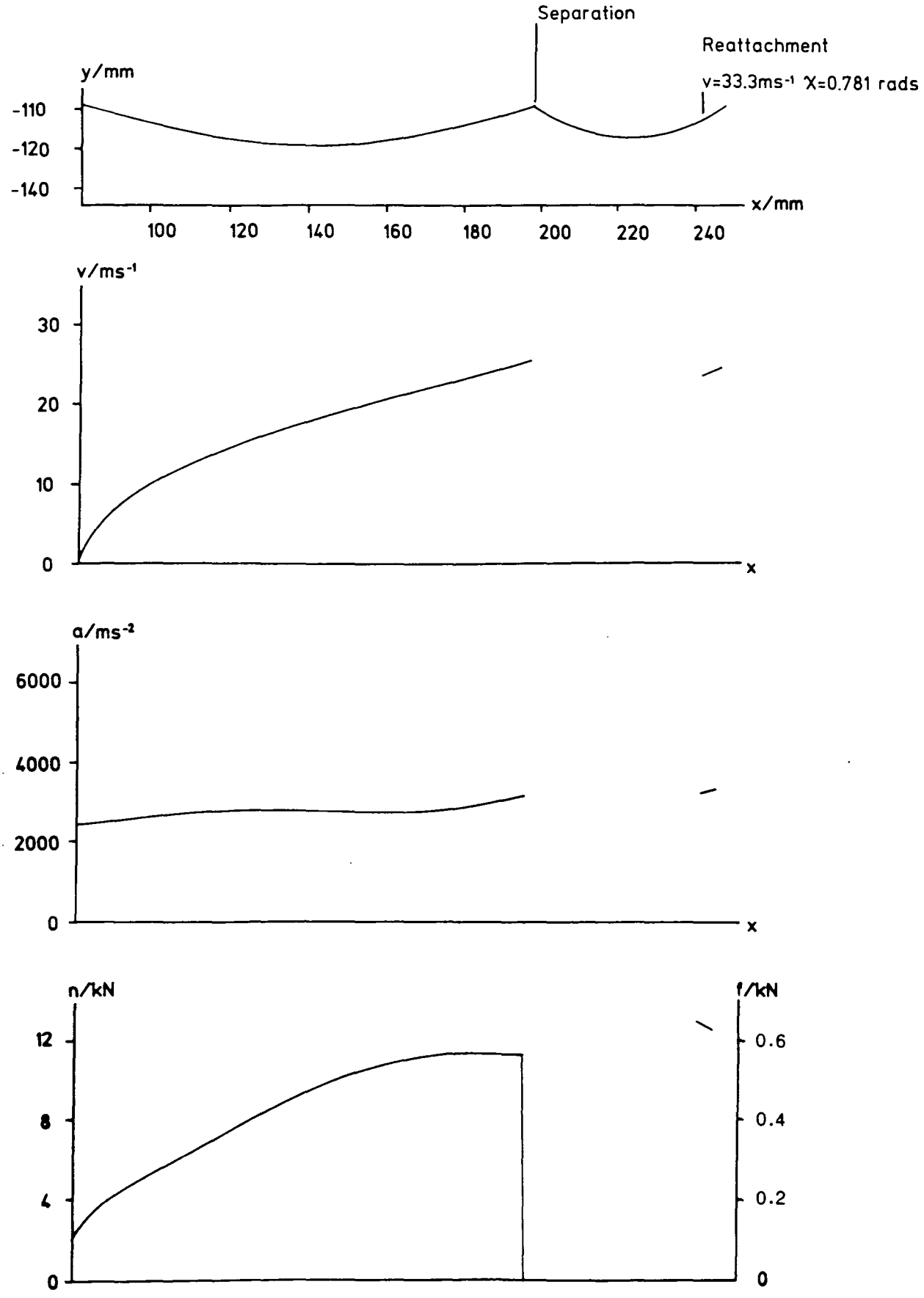

Figure 19

Action of Material in Breakring Impeller: Profile 4

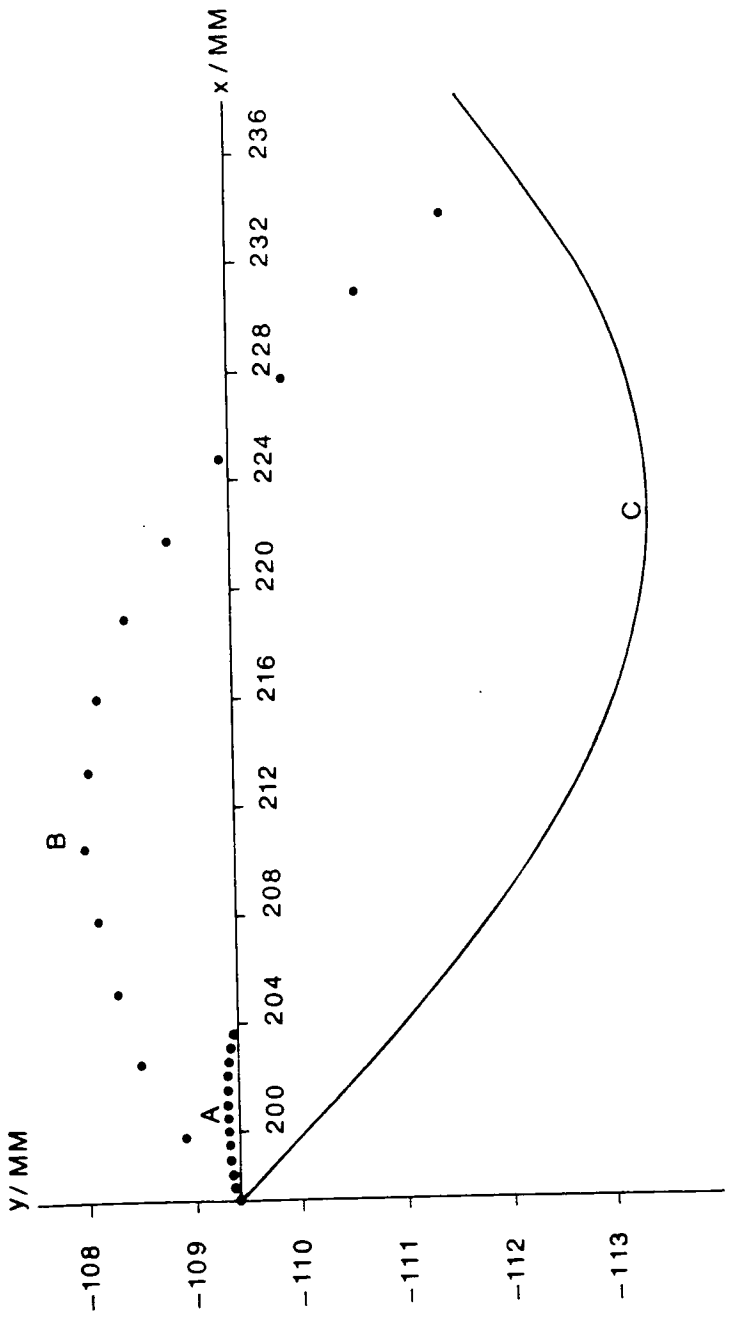

Figure 20

Relative Trajectories of Detached Particles

length 50 mm and 4 mm, approximated by half a wavelength of a sinusoidal curve. Points A represent the relative trajectory of the separated particle in the second test. The time interval between consecutive points is 2×10^{-5} seconds. Points B ($y > -109.4$ mm) represent the relative trajectory of the separated particle in the third test. Points B ($y < -109.4$ mm) show how the relative trajectory would develop if the surface contained the depression C. The time interval between consecutive points is 10^{-4} seconds.

It is seen from Figure 20, that reattachment occurs progressively further downstream as the two depressions develop. As a consequence of this shift, particles tend, generally, to reattach slightly downstream of the deepest point of the downstream depression.

In the fifth test, the upstream depression, of length 115 mm and depth 8 mm, was approximated by a full wavelength of a sinusoidal curve. The downstream region of the wear part was approximated by a straight line. The results, which are shown in Figure 21, indicate that the particle does not separate from the wear part surface. This was not unexpected since the wear part curvature, $d\rho/ds$, was low over the entire wear part length.

The wear part profile specified in the sixth test was identical to that of the third test. The coefficient of friction between the feed material and the wear part was set at 0.1. The results are shown in Figure 22. They indicate that the conditions at reattachment are not greatly affected by the increased coefficient of friction.

It was assumed in all tests that the feed material meets the upstream end of the wear part. It is clear that many particles meet the wear part downstream of that

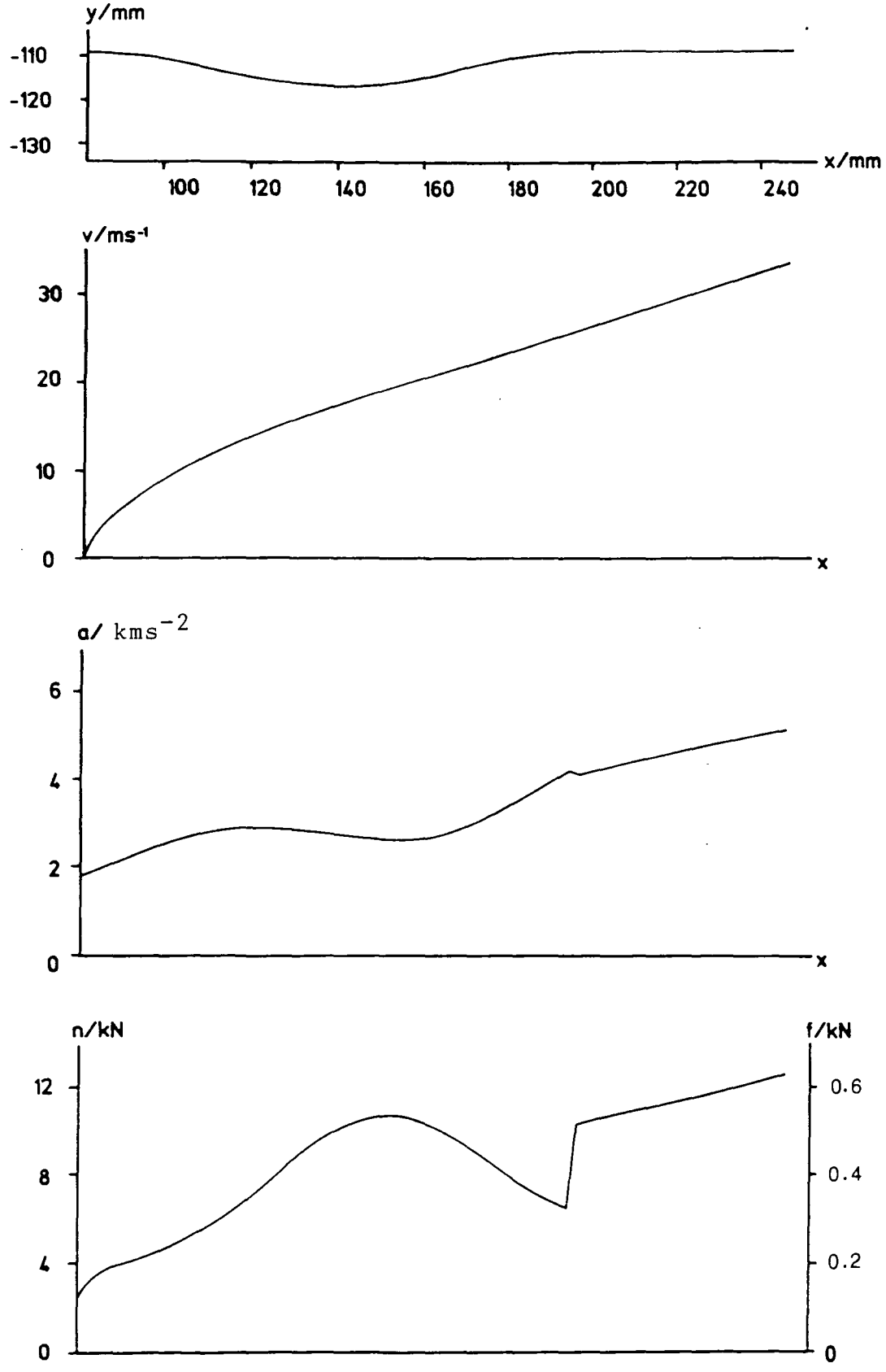

Figure 21

Action of Material in Breakring Impeller: Profile 5

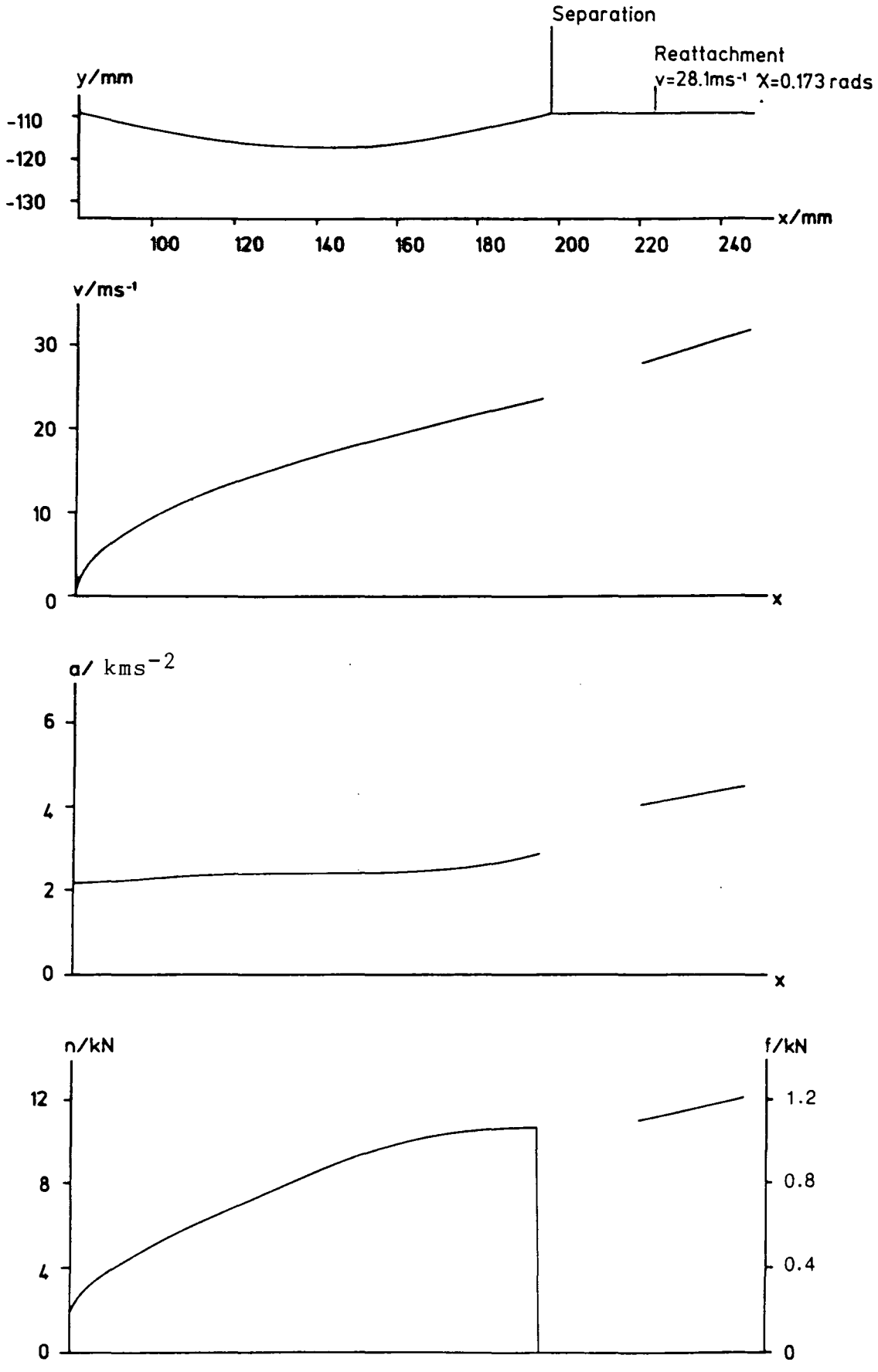

Figure 22

Action of Material in Breakring Impeller: Profile 6

point. The behaviour of those particles attaching at the upstream end was, however, considered to be of most interest, since it is such particles which exhibit the greatest speeds and are likely to be most responsible for the abrasion of the wear parts.

The analysis of Section 3.1 cannot be and was not applied to the complex, three-dimensional flow within the ports of the two-port impeller. It is believed, however, in the light of the six tests discussed above, that the third, downstream depression on the downstream wear part of the two-port impeller, as shown in Figures 24 and 25, results from the reattachment of material which separated at the second depression.

4. EXPERIMENTAL MODELLING OF BREAKRING OPERATION

4.1 Experimental program

An experimental programme was proposed, which comprised three parts, being the design and manufacture, in perspex, of a full scale model impeller, to be driven at full speed, the application of a surface flow visualisation technique to the study of air flow in the impeller and photography or stroboscopy of the flow of airborne material in the impeller. Cinematography of the flow, in the impeller, of light, non airborne material was considered but not planned in detail.

The design and manufacture of the impeller were completed successfully.

A trial was completed for the surface flow visualisation. Shortly after start up on the first full run, the impeller disintegrated. The precise cause of the disintegration was unknown and, because of other priorities, not investigated. Attention was paid instead to revision of the experimental programme. Options were strictly limited. It was chosen to continue work, using Impact Technology's demonstration Breakring crusher at the company's works in Eaglescliffe.

The surface flow visualisation was completed without further complication.

Photography of the flow of material in the impeller presented many difficulties. Viewing access into the impeller is limited to the feed inlet and exits. A stationary observer sees a useful view of the impeller

interior for only a small fraction of each revolution. In order to capture such a view on film, it is necessary to use synchronised or cine photography. Cinematography through the feed inlet was selected. Use of the prototype impeller introduced the possibility of filming the flow of solids. Landwehr and Pall (1987) mention the use of high speed cinematography in an investigation of the flow of peppercorns in a turbo-mill. They do not, however, discuss experimental technique in any detail.

Filming was undertaken on four occasions, with various degrees of success. Because of the lack of available expertise in high speed photography, a strict and formal programme of action was not defined. Instead, the course of each session was dictated by the results of the previous sessions. Illumination was provided by sunlight or arc-lamp and was, at best, less than ideal. Photography was thus undertaken under inadequate conditions because there was no alternative. Furthermore, due to limitations imposed on the use of the high speed camera, the photography was completed under intense time pressure. Experimental work was finally abandoned at the onset of winter.

4.2 Design of Model Impeller

The model impeller was based on the two-port prototype. It was driven at full speed, 1450 r.p.m., by a 30kW, 4 pole induction motor.

A cuboidal frame was fabricated from 80x80x5 mm box section tubing and bolted to the floor for stability. The bolts were arranged to hold in case of severe rotor imbalance. The motor was flange mounted, inside the frame, to 20 mm steel plate, bolted to the top face of the frame. 10 mm steel plate, bolted to the frame, formed a barrier around the impeller and was intended to

contain it in the event of disintegration. As a further precaution, a wall of sandbags was built around the rig. The motor switchgear was located outside the wall.

The model impeller is shown in Figure 23. The horizontal base was of 20 mm aluminium plate. To the base was fitted an aluminium distributor wedge, strengthened by two bulkheads. Two perspex side walls straddled the distributor wedge. Each side wall was mounted on two aluminium piers. A perspex top plate rested on the side walls and piers. An aluminium breakring was attached to the centre of the top plate. The assembly was fastened together by four pairs of M10 bolts. Each pair passed through the top plate and one pier and screwed directly into the base. The bolt holes were arranged so that the side walls could be displaced in 10 mm intervals. The port width was variable from 80 mm to 360 mm. 8 aluminium columns, of diameter 30 mm, lent further rigidity to the structure. Each column was bolted to the top plate by one M10 bolt and to the base by one M10 bolt. For clarity, all bolts and bolt holes are omitted from Figure 23. A mild steel boss was bolted to the base. This, also, is omitted from Figure 23. The maximum stress due to centrifugal loading in the side walls occurred at the fixed ends of the cantilever sections. It was reduced by use of sections tapering linearly to zero thickness at their free ends. 20 mm perspex was used. The maximum stress was 7.8 MPa, the factor of safety 10 and the free end deflection 3 mm.

The top plate was designed to be capable of bearing the centrifugal loading due to its own mass plus that of the side walls, piers, pillars and Breakring. 10 mm perspex was used. The maximum stress, at the feed opening, was 15 MPa and the factor of safely 5.

The maximum shear stress in the outer column fixing

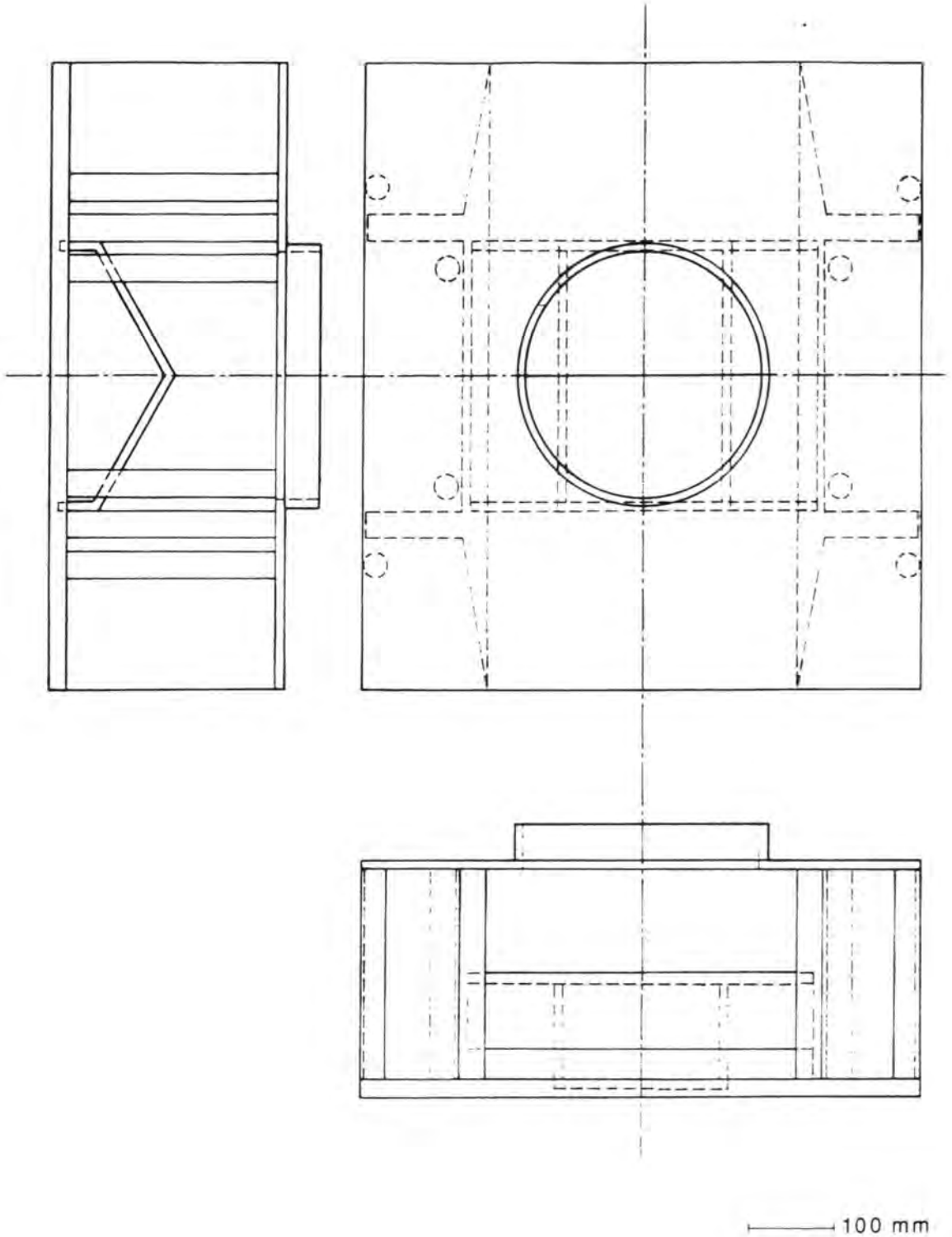

Figure 23

Model Impeller

bolts was 25 MPa and the factor of safety 9.

The maximum shear stress in the pier fixing bolts was 80 MPa and the factor of safety 3.

4.3 Surface flow visualisation on model impeller

4.3.1 Experimental method

The port width of the model impeller was set as that of the two-port prototype. Diesel oil and fluorescent powder paint were mixed in the ratio 3:1 by weight and applied liberally to the interior surfaces of the impeller (Settles, 1986). The impeller was run for five minutes, during which the mixture was blown by the air throughflow to form a pattern of streaks parallel to the surface streamlines.

The impeller was stripped down and the components examined.

4.3.2 Results

The surface pattern on the region of interest of each side wall consisted of uninterrupted horizontal streaks and suggested that the adjacent air flow contained no vortices which, in the presence of fines, might have lead to localised erosion. No record, photographic or otherwise, was made of the surface pattern.

The reliability of surface flow visualisation techniques, when applied to rotating systems, has been questioned. This matter is discussed in Section 4.5.2.

4.4 Demonstration crusher apparatus

Various apparatus was used during the course of experimental work on the demonstration crusher. The less familiar items are described below.

The demonstration crusher comprised a diesel driven Breakring supported on a skid mounted frame. Transmission was direct via a clutch. The impeller speed was controlled by altering the motor speed and was read directly from a tachometer. Throughout the work, the feed tube assembly was absent from the crusher, facilitating access to the impeller. A two-port impeller was used in all tests.

The cine camera used was a Red Lake Hycam K2054E 16 mm High Speed Motion Picture Camera, utilizing a rotating prism for optical compensation. The frame rate was variable from 100 to 11,000 pictures/second. Exposure was controlled by means of a rotating shutter. Throughout the work, the largest available shutter ratio, 1:2.5, was used. The shutter speed was given by the product of the shutter ratio and the reciprocal of the frame rate. The camera was started remotely with a hand held switch and stopped automatically when the end of the film was reached. It was equipped with a zoom lens and mounted on the lid of the crusher in a cradle of Dexion scaffolding.

Smoke was generated in the impeller by Smoke Cases, manufactured by Standard Fireworks Ltd. The Smoke Cases were mounted in bomb holders, one of which was mounted on each upper face of the specially modified distributor wedge. Smoke Cases burn for upto three minutes, producing dense grey smoke.

Sand and gravel were introduced to the impeller from two

hoppers, each of which contained a remotely operated trap door at its base. The hopper used in early tests had a diameter of 270 mm and that used in later tests a diameter of 80 mm. Both were approximately 400 mm in length. The hopper in use was mounted on the lid of the crusher in a cradle of Dexion scaffolding.

Three different films were used during the investigation. These were Ilford XI400 32 mm (400ASA), Kodak RAR 2498 16 mm (200ASA) and Eastman 7251 16 mm (400 ASA).

4.5 Surface flow visualisation on demonstration crusher

4.5.1 Experimental method

Two sets of worn wear parts were mounted in the impeller, which was then cleaned thoroughly. The anvil region of the crusher was hosed with water to prevent dust contaminating the wear part surfaces. A wash of diesel oil and fluorescent powder paint was mixed and applied to the wear part surfaces, as detailed in Section 4.3.1. The impeller was driven at 1450 r.p.m. for two minutes. In longer runs, the impeller picked up an excessive quantity of dust. The wear parts were removed from the impeller and photographed under ultraviolet light on Ilford XI400 film.

Figure 24 shows one downstream wear part. Figure 25 shows the upstream and downstream wear parts from the opposite port.

4.5.2 Results

The surface flow pattern on each downstream wear part consisted of largely uninterrupted streaks and again suggested that the adjacent air flow contained no vortices, which, in the presence of fines, might have lead to

Figure 24

Abraded Impeller Wear Part: Downstream

Figure 25

Abraded Impeller Wear Parts: Upstream and Downstream

localised erosion. The narrow dark region at the interface between the side and upper faces of each downstream wear part indicated the separation which resulted from convergence of the flows along the two surfaces.

The accuracy of these results is questionable, since the wash on the wear parts was subjected not only to aerodynamic but also centrifugal forces. The extent of any inaccuracy is unknown and cannot be measured. It is believed that if aerodynamic activity were responsible for the localised abrasion of the wear parts, then evidence of such activity, in the form of separation lines, would have been present in the region of interest, irrespective of the magnitude of centrifugal effects. This belief is confirmed by the presence, at the interface between the side and upper faces of the downstream wear part, of separation lines, indicating that aerodynamic effects were not obscured by centrifugal effects. The absence of separation lines or indeed of any evidence of turbulence in the region of interest is, therefore, regarded as a reliable indication that the localised abrasion of the wear parts is not connected with the air flow past them.

4.6 Cinematography on demonstration crusher

4.6.1 Experimental Method

4.6.1.1 Session 1

Two unused sets of wear parts were mounted in the impeller, the interior of which was then painted with dull white Smoothrite paint. The large hopper was positioned centrally and coaxially above the impeller feed inlet and filled with - 30 mm gravel, which had been sieved and washed to remove fines. The anvil region of the crusher was hosed with water to suppress dust. Weather

conditions were good. Illumination was by sunlight only. The camera was loaded with 225 feet of Kodak RAR 2498 film and mounted on the crusher. Zoom and focus were adjusted. The frame rate was set at 3000 pictures/second. At this frame rate, 225 feet of film runs for approximately 4.0 seconds, of which 1.0 - 1.5 seconds elapse while the camera accelerates. The impeller speed was set at 1450 r.p.m. The camera was started and, approximately one second later, the hopper opened. Once the camera had stopped, it was removed and unloaded.

This procedure was repeated with the frame rate set at 3500 pictures/second.

The hopper was removed. Two Smoke Cases were mounted in the impeller. The camera was loaded, mounted and adjusted as previously. The Smoke Cases were ignited. The impeller speed was again set at 1450 r.p.m. and the camera started. Once the camera had stopped, it was removed and unloaded.

The three films were reversal-processed.

The two films of the flow of gravel suffered from four faults. The large quantity of feed material obstructed the view into the impeller. Use of monochromatic film led to difficulties in interpretation of the results. The films were underexposed. A large region of the impeller interior was in shadow for the greater part of each revolution. Comparison of the two films revealed that the better combination of exposure and sharpness was achieved at a frame rate of 3000 picture/second. This frame rate was selected for all future filming sessions.

The film of the flow of smoke was badly processed.

4.6.1.2 Session 2

The flow of gravel within the impeller was filmed by a technique similar to that of the first session but incorporating the following alterations. The narrower feed hopper was used and was filled with -20 mm gravel. The camera was loaded with 100 feet, the longest available length, of faster Eastman 7251 colour film and repositioned on the crusher so as to view the impeller interior when the region in shadow was smallest. Since, at 3000 pictures/second, 100 feet of film runs for only 2.4 seconds, the camera was not started until the feed material was seen to leave the hopper.

This procedure was repeated with a second identical film.

Much improved results were obtained on this occasion. The above type and length of film was selected for all future filming sessions.

It was observed that due to the reduced quantity of feed material used, contact been feed particles and the breakring was low. This is in contrast to the condition achieved during crushing operation, when there is chocked flow in the breakring.

4.6.1.3 Session 3

The flow of smoke in the impeller was filmed by the technique of the first session. Weather conditions were poor. Illumination was supplemented by a 1200 W tungsten halogen arc lamp.

The film was reversal-processed.

Lighting was inadequate and the film consequently under-exposed.

4.6.1.4 Session 4

The impeller was fitted with one unused set of wear parts and one severely worn set and the interior painted with Smoothrite. Weather conditions were good. Illumination was by sunlight only.

The flow of smoke within the impeller was filmed by the procedure of the first session.

The flow of gravel was filmed by the technique of the second session. On this occasion, the feed hopper was mounted eccentrically above the impeller feed opening so as to direct the feed material against the breakring inner wall and thus more closely reproduce the condition achieved during crushing operation. This arrangement is shown in Figures 26 and 27. The procedure was repeated with the hopper filled with builder's sand.

The three films were reversal-processed.

The film of the flow of smoke was generally under-exposed. In particular, the downstream end of each impeller port was in shadow and the smoke in that region indiscernible. The films of the flows of sand and gravel were obscured by an unidentified dark object which blocked all but the right hand quarter of each frame.

4.6.2 Results

As indicated in Sections 4.5.1.1 to 4.5.1.4, only the films exposed in the second session showed clearly the

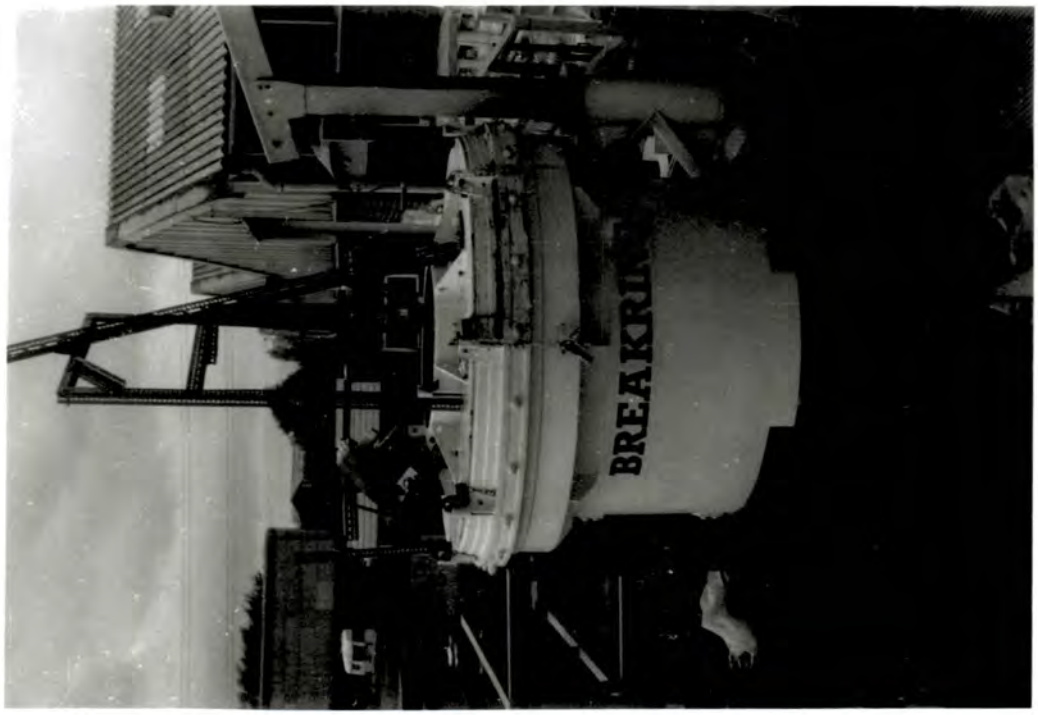

Figure 26

Demonstration Crusher Arrangement

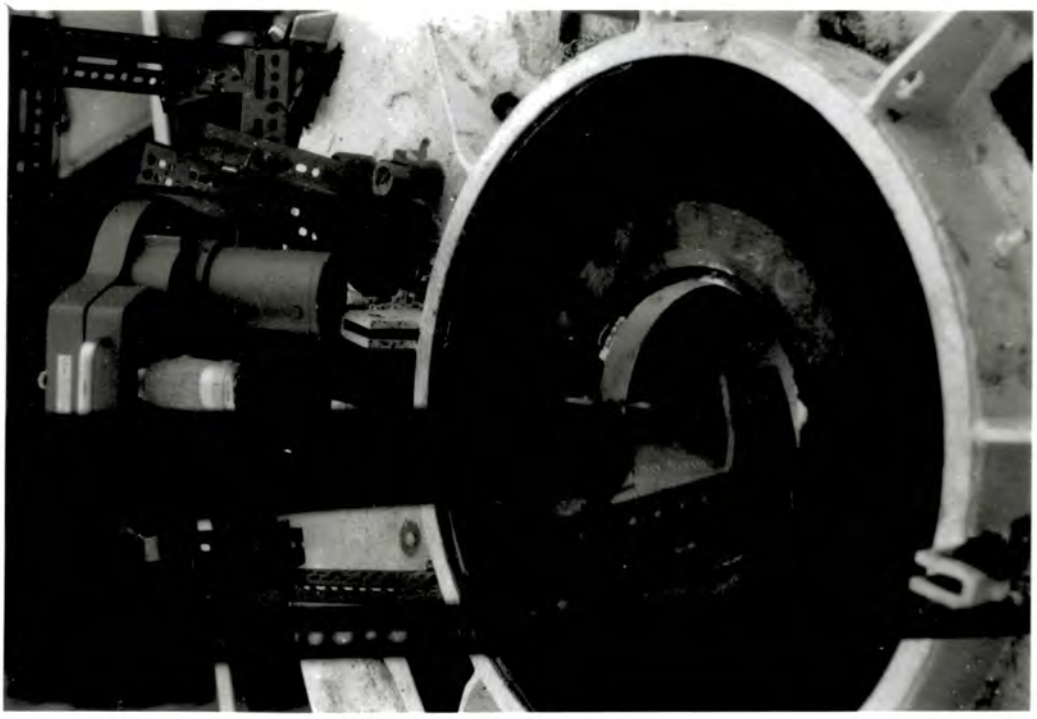

Figure 27

Camera and Feed Arrangement

behaviour of material within the impeller. No action could be seen in these two films, which might obviously have given rise to localised abrasion of the impeller wear parts. In particular, the films did not aid verification of the results of the computer simulation described in Section 4.3, which predicted separation and reattachment only for an impeller containing worn wear parts.

Material attached to the forward facing side walls was seen generally to travel horizontally outwards towards the port exit. Many particles fell into the impeller without being accelerated in the breakring and thus, when picked up by either of the forward facing side walls, had inwardly directed components of velocity relative to the wall. These particles generally travelled a short distance upstream along the wall before reversing and accelerating outwards towards the port exit. Some particles, however, travelled as far as the back facing wall of the opposite exit port, from which they soon detached. These conditions are unlikely to be encountered during crushing operation since the choked flow in the Breakring rotates at near impeller speed and has only a low relative velocity.

At the region of each impeller side wall, such that the radius to the axis of rotation was approximately perpendicular to the wall, static layer of material built up under the action of frictional force.

An attempt was made to produce positive prints from the films of the second session. Since, however, the transparencies were reversal-processed (to permit cine projection), it was necessary to produce, first of all, negative transparencies and, from these, positive prints. The loss of picture quality encountered at both stages of this operation together with poor quality of

the originals due to poor illumination, the motion of the impeller and the graininess of the high speed film meant that results were unrecognizable and are hence not included in this report.

The seven films of the other sessions were unsuccessful for reasons discussed previously.

5. DISCUSSION

The results of Section 2.3 show the ideal performance of the Breakring.

The results of Section 3.3 indicate the mechanism responsible for the localised abrasion of the impeller wear parts. Three factors not discussed in Section 3.3 confirm the accuracy of the mechanism indicated. Firstly, no downstream depression was formed on the wear part when, as for certain feed materials and earlier impeller designs, the upstream depression was similar in profile to a full sine wave. The results of Section 3.3 predict that separation and detachment do not occur for such an upstream depression. Secondly, each downstream depression had a steeper downstream face than upstream face. Such a depression would be formed if material were to impact the surface at a shallow angle. Thirdly, smooth, ripple-like surface profiles, similar to those of the worn wear parts, have been observed on exit chutes of screens clearly carrying only non-airborne material.

As stated in Section 1, the localised abrasion of the wear parts was especially severe when the feed contained a large fraction of fines. The significance of fines can also be attributed to the mechanism indicated in Section 3.3, as follows: The model of Section 3.2 predicts, accurately, the action only of point masses in the absence of aerodynamic forces. In practice, the feed comprises a spread of particle sizes. The largest particles do not follow surface irregularities faithfully or separate and reattach as predicted. The finest particles are influenced primarily by aerodynamic forces and also do not behave as predicted. In between, there is, presumably, a size of particle which most closely

satisfies the point mass and low aerodynamic drag conditions and which acts in a manner closest to that predicted by the model of Section 3.2 and separates and reattaches as described. It is supposed that the fine material, for which the localised abrasion of the wear pats is most severe, contains many particles of this size.

The limited flow visualisation undertaken produced no evidence of air flow, with which the localised abrasion might be connected. Also no cause was identified for such flow. Some relative rotation of the air in the impeller port, contrary to the direction of impeller rotation, as has been observed in the impellers of centrifugal compressors (Eck, 1973), might be expected. Such rotation, however, when superimposed on the main airstream, would tend to reduce the relative air speed in the vicinity of the forward facing wear parts and hence reduce erosion by airborne material. The possibility of pressure waves being reflected from the staggered anvils into the impeller ports, where they might interact to form standing waves, carrying abrasive material, was also suggested. This theory was considered far-fetched and consequently discarded.

As stated in Section 1, the wear phenomenon in question has not been reported previously. It has emerged from recent conversation with designers of other VSIs, however, that similar wear patterns have been observed in the impellers of machines resembling that shown in Figure 1. The impeller of such a machine is open. That of the Breakring is enclosed. The airflows past the wear parts of the two impellers are, therefore, unlikely to be similar. The similarity between the two wear patterns would seem to confirm that the abrasion is independent of the airflow.

In the light of the above, it seems unnecessary to continue the experimental program. Much was learned from the work completed, which though not of direct interest to the topic under consideration, is still worth noting. It is apparent that the original model impeller design was inadequate. In particular, it seems that perspex was unsuitable as a structural material in this application. Also, it was perhaps unwise to build a variable-geometry model at the first attempt. It is suggested that, if a new model impeller were to be manufactured, then it should have a robust and self-supporting fixed-geometry base and frame of steel or aluminium and top and side walls of perspex plate, mounted in the frame in a manner permitting ease of replacement. With such a construction, it would be possible to observe the flow of smoke as intended with the original model but without the need for great care or the threat of disintegration of the impeller.

The impeller could be mounted in a laboratory, as it was previously. If it were to be mounted in the prototype crusher body with the cover plate and feed tube fitted, then the flow of rock could be filmed successfully and accurately. In this instance, it would be necessary to use aluminium or steel plate for the impeller walls along which the material slides. Once the other, perspex impeller walls became damaged, they could be replaced with facility. The cover plate of the crusher would, of course, require modification to provide illumination and viewing access. Further attention would need to be paid to illumination. In view of the results already achieved at Eaglescliffe, it seems likely that at midsummer, sunlight might be adequate for high speed photography, since perspex impeller walls would produce no shadows. The employment of powerful direct current artificial lighting would also be worthy of investigation. Finally, it should be borne in mind, that the airflow patterns observed in the impeller when it is

running empty are likely to be different from those present when it is passing rock.

6. CONCLUSIONS AND SUGGESTIONS FOR FURTHER WORK

6.1 Conclusions

The following conclusions were drawn from the results of this work.

1 The analysis and computation of Breakring performance, based on integration of the governing differential equation of motion of a single particle in the Breakring impeller, though adequate for simple impeller wear part profiles, are of limited applicability. There does not appear to be much scope or need for development of this method.

2 The analysis and computation of the action of a single particle in the Breakring impeller, based on solution of the equations of motion of the particle on the segmentised wear part profile, is flexible and powerful.

3 The surface flow visualisation in the rotating impeller was shown probably to be reliable. It also, however, appears to possess little scope or need for development.

4 Cinematography of the flow of smoke and solids in the Breakring impeller is problematic but with modification could yield useful results.

5 The localised abrasion of the wear parts of two- and six- port impellers results probably from the impact of feed material reattaching to the wear part following separation from the downstream end of the depression formed on the wear part by the initial impact of material after entry to the impeller. There is no reason to believe that airborne fines are responsible for this abrasion.

6.2 Suggestions for further work

The possibilities for further work are virtually limitless. Three are suggested below.

1 Continuation of cinematography of the flow of smoke and solids in a modified model impeller.

2 Development of mathematical modelling to account for three-dimensional material flow in the impeller and the effects of finite particle size.

3 Examination of the conditions governing the shape of the impeller wear part upstream depression.

In order for further work to be worthwhile, precise specification of its objectives would be necessary.

7 APPENDICES

7.1 Appendix 1

Computer Program: Breakring Performance

```
C   PROGRAM ROCK COMPUTES VELOCITY,ACCELERATION AND FRICTIONAL AND NORMAL
C   FORCES IN PORT OF BREAKRING
C
C   POSITION DEPENDENT NUMERICAL ANALYSIS
C   ANALYTICAL EVALUATION OF POWER
C
C   PRINTED OUTPUT FROM ROCK ASSIGNED TO UNIT 1 BECAUSE TEAPACK SUBROUTINE
C   OUTPUT ASSIGNED TO UNIT 6
C
C   TO RUN PROGRAM ON NUMAC MTS
C   RUN *FORTRANVS SCARDS=ROCK
C   RUN -LOAD+ES08:TPCOM 5=ROCKD.DTA 1=-P 6=-Q 2=X.DTA
C   COPY -P
C
      EXTERNAL FSV
      REAL PARRAY(100,100),AARRAY(100,100),VARRAY(100,100),COORDS(100,2)
     &,CMN(12)
      COMMON/PAR/CF,A,AV,VIN,CT,ST,TOL,SP,AC,AO,B
      DATA PI/3.1415926539/
      NZ=0
      IMAX=0
C
C   READ IN DATA
C
      READ(5,*)NC,NANG,NS,A,B,AO,RPM,VIN,DMIN,DMAX,CFMIN,CFMAX,RMF
     &,NA,TOL
C
C   NC    :NUMBER OF COEFFICIENTS OF FRICTION
C   NANG  :NUMBER OF PORT ANGLES
C   NS    :NUMBER OF POINTS ALONG PORT
C   A     :RADIUS OF ACCELERATOR PLATE
C   B     :PORT LENGTH
C   AO    :RADIUS OF ANVIL SURFACE
C   RPM   :IMPELLER ROTATIONAL SPEED(R.P.M.)
C   VIN   :ANGLE BETWEEN PORT AND RADIAL
C   DMIN  :MINIMUM PORT ANGLE
C   DMAX  :MAXIMUM PORT ANGLE
C   CFMIN:MINIMUM COEFFICIENT OF FRICTION
C   CFMAX:MAXIMUM COEFFICIENT OF FRICTION
C   RMF   :TOTAL MASS FLOW RATE
C   NA    :NUMBER OF PORTS ON IMPELLER HEAD
C   TOL   :TOLERANCE ON ACCURACY OF ROOT SEARCH AND INTEGRATIONS
C
C   ALL DIMENSIONS IN SI UNITS
C
C   CHECK ANGLE OF ARM IS IN RANGE -90 TO +90 DEGREES
C
      IF(DMAX.GT.90.0D 00)THEN
        DMAX=90.0D 00
        ELSE IF(DMIN.LT.-90.0D 00)THEN
          DMIN=-90.0D 00
        ELSE
      ENDIF
      ANGMAX=DMAX*PI/180.0D 00
      ANGMIN=DMIN*PI/180.0D 00
C
      AV=PI*RPM/30.0E 00
C
      IF(NS.EQ.1)NS=2
C

      NCI=NC-1
      IF(NCI.LE.0)THEN
        CFINT=0.
        GO TO 100
      ELSE
      CFINT=(CFMAX-CFMIN)/NCI
      END IF
  100 NANGI=NANG-1
      IF(NANGI.LE.0)THEN
        ANGINT=0.
        GO TO 101
      ELSE
        ANGINT=(ANGMAX-ANGMIN)/NANGI
      END IF
  101 NSI=NS-1
      BINT=B/NSI
C
C   PRINT OUT BASIC DATA
C
      WRITE(1,200)
      WRITE(1,201)A,B,RPM,VIN,DMIN,DMAX,CFMIN,CFMAX,AO,RMF
```

```
C
CC   LOOP ON FRICTION COEFFICIENTS
C
      DO 10 I=1,NC
      I1=I-1
      CF=CFMIN+I1*CFINT
C
CC   LOOP ON PORT ANGLES
C
      DO 20 J=1,NANG
      J1=J-1
      ANG=ANGMIN+J1*ANGINT
      CT=COS(ANG)
      ST=SIN(ANG)
      AC=A*(CT-CF*ST)
      WRITE(1,207)
C
CC   LOOP ON NUMBER OF POINTS ALONG GUIDE
C
      DO 30 K=1,NS
      K1=K-1
      SPI=SP
      SP=K1*BINT
      IF(K.EQ.1)THEN
      VP=VIN
      GO TO 40
      ELSE
      ENDIF
C
CC   COMPUTATION BY RUNGE-KUTTA-FEHLBERG OF SPEED AT DISPLACEMENT SP
C    IVODE:TEAPACK SUBROUTINE
C
      N=1
      IFMLA=1
      IND=0
      LIST=0
      TOLI=10000*TOL
      DO 31 NCMN=1,10
      CMN(NCMN)=0.E0

   31 CONTINUE
      CALL IVODE(FSV,N,SPI,VP,SP,TOLI,IFMLA,IND,CMN,LIST)
      IF(IND.LT.0)THEN
        WRITE(1,202)
        CALL ERR(PARRAY(I-1,J),VARRAY(I-1,J),AARRAY(I-1,J),
     &           PARRAY(I,J),  VARRAY(I,J),  AARRAY(I,J),
     &           COORDS,NC,NANG,I,J,NZ,IMAX)
        GO TO 20
      ELSE
      ENDIF
   40 CONTINUE
C
CC   CALCULATION OF ACCELERATION(AP),FRICTION FORCE(FF),NORMAL FORCE(FN),
C    CHECK RATIO(R) AT DISPLACEMENT (SP) ALONG GUIDE
C
      IF(VP.LT.0.)THEN
        WRITE(1,203)
        CALL ERR(PARRAY(I-1,J),VARRAY(I-1,J),AARRAY(I-1,J),
     &           PARRAY(I,J),  VARRAY(I,J),  AARRAY(I,J),
     &           COORDS,NC,NANG,I,J,NZ,IMAX)
        GO TO 20
      ELSE
      ENDIF
      AP=AV*AV*(AC+SP)-2.*CF*AV*VP
      FF=AV*AV*(A*CT+SP)-AP
      IF(FF/ABS(AP).LT.(-1000*TOL))THEN
        WRITE(1,*)'FF=',FF
        WRITE(1,204)
        CALL ERR(PARRAY(I-1,J),VARRAY(I-1,J),AARRAY(I-1,J),
     &           PARRAY(I,J),  VARRAY(I,J),  AARRAY(I,J),
     &           COORDS,NC,NANG,I,J,NZ,IMAX)
        GO TO 20
      ELSE IF((FF.LT.0).AND.(FF/ABS(AP).GT.(-1000*TOL)))THEN
        WRITE(1,205)
      ELSE
      ENDIF
      FN=A*AV*AV*ST+2.0*AV*VP
      IF(FN.LE.0.0)THEN
        WRITE(1,206)
        CALL ERR(PARRAY(I-1,J),VARRAY(I-1,J),AARRAY(I-1,J),
     &           PARRAY(I,J),  VARRAY(I,J),  AARRAY(I,J),
     &           COORDS,NC,NANG,I,J,NZ,IMAX)
        GO TO 20
      ELSE
      ENDIF
      R=FF/FN
C
CC   PRINT OUT RESULTS AT DISPLACEMENT SP
C
      DANG=ANG*180/PI
      WRITE(1,201)CF,DANG,SP,VP,AP,FF,FN,R,TOL
C
CC   VELOCITIES AT PORT EXIT
C    VOR  :RELATIVE OUTPUT VELOCITY OF MASS IN GUIDE
C    VX   :ABSOLUTE EXIT VELOCITY (X COMPONENT)
C    VY   :ABSOLUTE EXIT VELOCITY (Y COMPONENT)
C    VOUT:ABSOLUTE EXIT VELOCITY
C
C    EXIT FLOW DIRECTIONS
C    DANGEX:EXIT VELOCITY DIRECTION RELATIVE TO PORT DIRECTION(DEGREES)

C    DAP    :ANVIL ORIENTATON FOR NORMAL IMPACT(DEGREES)
C
   30 CONTINUE
      VOR=VP
      VX=A*AV*ST+VOR
      VY=AV*(B+A*CT)
      VOUT=SQRT(VX*VX+VY*VY)
      DANGEX=180.0*ATAN(VY/VX)/PI
      CALL ANVIL (VX,VY,VOR,RAP)
      DAP=DANGEX-180.*RAP/PI
      WRITE(1,208)
      WRITE(1,201)VOR,VX,VY,VOUT,DANGEX,DAP
```

```
C
C   ANALYTICAL EVALUATION OF POWER CONSUMPTION
C
      POWER=RMF*AV*AV*(B*B+2*A*B*CT+A*ST*(VOR-VIN)/AV)
C
C   STORAGE OF PERFORMANCE DATA
C
      PARRAY(I,J)=POWER
      VARRAY(I,J)=VOUT
      AARRAY(I,J)=DAP
C
C   PRINT OUT OVERALL PERFORMANCE PARAMETERS
C
      WRITE(1,209)
      WRITE(1,201) A,B,RPM,RMF,VIN,CF,POWER,DANG
C
   20 CONTINUE
   10 CONTINUE
C
C   INPUT OF RESULTS TO FILE DATA.DTA
C
      WRITE(2,*)NC,CFMIN,CFINT,NANG,ANGMIN,ANGINT,NZ,
     &((PARRAY(I,J),J=1,NANG),I=1,NC),
     &((VARRAY(I,J),J=1,NANG),I=1,NC),
     &((AARRAY(I,J),J=1,NANG),I=1,NC),
     &((COORDS(I,J),J=1,2),I=1,NZ)
C
  200 FORMAT(1HO,T4,'RADIUS',T16,'PORT LENGTH',T29,'R.P.M.',T40,
     1'IN.VEL.',T53,'MIN.ANG.',T63,'MAX.ANG.',T76,'MIN.MU',T88,
     2'MAX.MU.',T100,'ANVIL R.',T113,'MASS FLOW'/)
  201 FORMAT(1H ,10G12.4)
  202 FORMAT(1H ,'INTEGRATION FAILED'/)
  203 FORMAT(1H ,'PARTICLE STOPS IN PORT'/)
  204 FORMAT(1H ,'FRICTION FORCE REVERSED - JUMP OUT OF LOOP'/)
  205 FORMAT(1H ,'FRICTION FORCE APPROACHES NEGATIVE'/)
  206 FORMAT(1H ,'NORMAL FORCE REVERSED',/)
  207 FORMAT(1HO/1HO,T4,'MU',T17,'IN.ANG.',T28,'DISTANCE',
     1T40,'VELOCITY',T52,'ACCEL.',T65,'F.FORCE',T77,'N.FORCE',
     2T89,'C.RATIO',T100,'TOLERANCE'/)
  208 FORMAT(1H /,T5,'REL.EX.V.',T17,'ABS.X-V.',T29,'ABS.Y-V.',
     1T41,'ABS.EX.V.',T53,'EXIT ANG.',T65,'ANVIL ANG.'/)
  209 FORMAT(1H /,T4,'RADIUS',T16,'PORT LENGTH',T29,'R.P.M.',T41,
     1'MASS FLOW ',T52,'INPUT V.',T64,'MU',T76,'POWER',
     2T89,'ARM ANG.'/)
      STOP
      END
C
C   ANVIL EVALUATES ORIENTATION OF ANVIL PLATES TO TANGENT OF ANVIL RING
C   FOR NORMAL IMPACT
C
      SUBROUTINE ANVIL(VX,VY,VOR,RAP)
      COMMON/PAR/CF,A,AV,VIN,CT,ST,TOL,SP,AC,AO,B
      VOS=VX*VX+VY*VY
      CA=VOR*(A*CT+B)
      FAC=VOS*(AO*AO-(A*A+B*B+2.0*A*B*CT))
      TIMP=(SQRT(CA*CA+FAC)-CA)/VOS
      RAP=ATAN((VY*TIMP-A*ST)/(VX*TIMP+A*CT+B))
      RETURN
      END
C
      SUBROUTINE FSV(N,S,V,VPRIME)
C   FSV DEFINES GOVERNING DIFFERENTIAL EQUATION
C   IN FORM dV/dS=f(V,S),WHERE VPRIME=dV/dS
      COMMON/PAR/CF,A,AV,VIN,CT,ST,TOL,SP,AC,AO,B
      VPRIME=AV*AV*(AC+S)/V-2.*CF*AV
      RETURN
      END
C
      SUBROUTINE FMLA(FSV,N,XS,US,USP1,ERREST,CMN)
      REAL XS,US(N),USP1(N),ERREST(N),CMN(12)
      EXTERNAL FFU,JFFU
      RETURN
      END
C
      SUBROUTINE ERR(P,V,A,PP,VV,AA,COORDS,NC,NANG,I,J,NZ,IMAX)
C   UNDEFINED POINTS ON (I,J) PLANE ASSIGNED POWER,SPEED AND ANGLE VALUES
C   OF LAST DEFINED POINT ON SAME ROW
C
C   IMAX   :I-COORDINATE S.T. LINE I=IMAX CONTAINS AT LEAST ONE UNDEFINED POINT
C   J-1    :J-COORDINATE OF LAST DEFINED POINT ON LINE I=IMAX
C   NZ     :NUMBER OF LINES I=CONST CONTAINING AT LEAST ONE UNDEFINED POINT
C   COORDS:COORDINATES OF POINTS(IMAX,J-1)
C
      REAL COORDS(100,2)
      IF(I.GT.IMAX)THEN
        IMAX=I
        NZ=NZ+1
        COORDS(NZ,1)=IMAX
        COORDS(NZ,2)=J-1
      ELSE
      END IF
      PP=P
      VV=V
      AA=A
      RETURN
      END
```

7.2 Appendix 2

Computer Program: Contour Production

```
C          file PLOT plots contours of
C
C          1.power requirement
C          2.absolute particle speed at port exit
C          3.anvil incination to circumfrential for normal impact
C
C          against
C
C          1.coefficient of friction between particle and'port lining
C          2.port inclination to radial
C
C          for device of 'BREAKRING' type
C
C          data evaluated by file ROCK and stored in file DATA.DTA
C-------------------------------------------------------------------------------
C
C          to run program on numac mts
C          RUN *FORTRANVS SCARDS=PLOT
C          RUN -LOAD+*GHOST80 2=DATA.DTA 9=-PLOT.PDF
C
C          to view resulting graph
C          RUN *PLOTSEE
C
C-------------------------------------------------------------------------------
C
      EXTERNAL COT
C          PARRAY:power data
C          VARRAY:speed data
C          AARRAY:anvil inclination data
C          CLEVLS:contour levels
C          COORDS:coordinates of limiting points of device performance

      REAL PARRAY(100,100),VARRAY(100,100),AARRAY(100,100),
     &     ZARRAY(100,100),CLEVLS(20),     COORDS(100,2)
      CHARACTER*23 MU
      CHARACTER*19 THETA
      CHARACTER*11 HEAD1
      CHARACTER*14 HEAD2
      CHARACTER*14 TITLE
C
      DATA PI/3.14159265395/
C
C          reading of data from DATA.DTA
C
      READ(2,*)NC,CFMIN,CFINT,NANG,ANGMIN,ANGINT,NZ,
     &((PARRAY(I,J),J=1,NANG),I=1,NC),
     &((VARRAY(I,J),J=1,NANG),I=1,NC),
     &((AARRAY(I,J),J=1,NANG),I=1,NC),
     &((COORDS(I,J),J=1,2),I=1,NZ)
C
      CALL PAPER(1)
      CALL PSPACE(0.4,0.95,0.25,0.95)
C
C          setting of axis limits
C
      XMIN=CFMIN
      XMAX=CFMAX+NC*CFINT
      YMIN=ANGMIN*180/PI
      YMAX=(ANGMIN+NANG*ANGINT)*180/PI
C     CALL AXOBIG(XMIN,YMIN)
      CALL MAP(XMIN,XMAX,YMIN,YMAX)
      CALL AXES
C
      CALL LINCOL(2)
      IF(XMIN.LT.1E-2)THEN
        XLIM1=1E-2
        ELSE
          XLIM1=XMIN
      ENDIF
      CALL GRAPHX(COT,XLIM1,XMAX)
C
C-------------------------------------------------------------------------------
C
    1 WRITE(6,*)'POWER,PARTICLE VELOCITY,ANVIL INCLINATION OR END?'
      WRITE(6,*)'1,2,3 OR 4?'
      READ(5,*)NO
C
C          transfer of power,velocity or anvil inclination data to zarray
C
      IF(NO.EQ.1)THEN
        DO 1000 I=1,NC
        DO 1001 J=1,NANG
        ZARRAY(I,J)=PARRAY(I,J)
1001    CONTINUE
1000    CONTINUE
        ELSE IF(NO.EQ.2)THEN
          DO 2000 I=1,NC
          DO 2001 J=1,NANG
          ZARRAY(I,J)=VARRAY(I,J)
2001      CONTINUE
2000      CONTINUE
          ELSE IF(NO.EQ.3)THEN
            DO 3000 I=1,NC
            DO 3001 J=1,NANG
            ZARRAY(I,J)=AARRAY(I,J)
3001        CONTINUE
3000        CONTINUE
            ELSE IF(NO.EQ.4)THEN
              GOTO4000
              ELSE
                GOTO1
      ENDIF
```

```
C
C
      CALL SLEVL(NO,NC,NANG,ZARRAY,CLEVLS)
C
C
      IMIN=1
      IMAX=1
      JMIN=1
      JMAX=1
C
      XNC=NC
      XNANG=NANG
C
      CALL FULL
      CALL MAP(1.,XNC,1.,XNANG)
C
      DO 400 N=1,NZ
C
C           CONOTA(0) disables contour line numbering
C
      IF((N.EQ.6).OR.(N.EQ.32).OR.(N.EQ.62))THEN
        CALL CONOTA(1)
        ELSE
          CALL CONOTA(0)
      ENDIF
C
C           determination of region for which CONTRA to be called
C
      IMIN=IMAX
      IMAX=COORDS(N,1)
      JMAX=COORDS(N,2)
C
C           determination of window
C
      XIMIN=IMIN
      XIMAX=IMAX
      XJMIN=JMIN
      XJMAX=JMAX
C
      CALL WINDOW(XIMIN,XIMAX,XJMIN,XJMAX)
      CALL CONTRA(ZARRAY,IMIN,IMAX,100,JMIN,JMAX,100,CLEVLS,1,20)
  400 CONTINUE
C
C-------------------------------------------------------------------------------
C
C           annotation of plot
C
C           1.labelling of axes
C
      CALL MAP(0.,10.,0.,10.)
      MU='Coefficient of friction'
      THETA='Port angle(degrees)'
      CALL PLOTCS(3.5,-1.,MU)
      CALL PLOTCS(-1.2,10.5,THETA)
C
C           2.labelling of contours
C
      CALL PSPACE(0.,1.,0.,1.)
      HEAD1='CONTOUR NO.'
      IF(NO.EQ.1)THEN
        HEAD2='POWER(W)          '
        TITLE='POWER CONTOURS'
        ELSE IF(NO.EQ.2)THEN
          HEAD2='SPEED(M/S)      '
          TITLE='SPEED CONTOURS'
          ELSE
            HEAD2='ANGLE(DEGREES)'
            TITLE='ANGLE CONTOURS'
      ENDIF
C
C           column headings
C
      CALL PLOTCS(0.7,9.83,HEAD1)
      CALL PLOTCS(1.9,9.83,HEAD2)
C
C           contour numbers and heights
C
      DO 500 I=1,20
      IVALUE=I
      YLOC=9.5-0.35*I
      CALL PLOTNI(0.8,YLOC,IVALUE)
      CALL PLOTNE(2.0,YLOC,CLEVLS(I),4)
  500 CONTINUE
      CALL CTRMAG(20)
      CALL LINCOL(4)
      CALL PLOTCS(4.,10.5,TITLE)
      CALL FRAME
      CALL GREND
 4000 STOP
      END
```

```
C
CCC-----------------------------------------------------------------------
CCC
CCC         subroutine SLEVL evaluates contour levels

      SUBROUTINE SLEVL(NO,NC,NANG,PARRAY,CLEVLS)
      REAL PARRAY(100,100),CLEVLS(20)
C
CCC         determination of maximum and minimum contour heights

      XMAX=0
      XMIN=10000000
      DO 100 I=1,NC
      DO 200 J=1,NANG
      IF(PARRAY(I,J).GT.XMAX)XMAX=PARRAY(I,J)
      IF((PARRAY(I,J).LT.XMIN).AND.(PARRAY(I,J).GT.-99))XMIN=PARRAY(I,J)
  200 CONTINUE
  100 CONTINUE
C
CCC         determination of contour levels

      XINT=(XMAX-XMIN)/19
      IF(NO.EQ.1)THEN
        XMIN=1E3*INT(XMIN/1E3)
        XINT=500*INT(0.5+XINT/500)
        ELSE IF(NO.EQ.2)THEN
          XMIN=INT(XMIN)
          XINT=0.1*INT(10*XINT)
          ELSE
          ENDIF
      DO 300 I=1,20
      CLEVLS(I)=XMIN+(I-1)*XINT
  300 CONTINUE
      RETURN
      END
C
CC-----------------------------------------------------------------------
C
      FUNCTION COT(X)
C
CCC         COT(X) gives function f(x)=tan-1(1/x)
C
      DATA PI/3.14159265395/
      COT=ATAN(1/X)*180/PI
      RETURN
      END
```

7.3 Appendix 3

Computer Program: Action of Material in Breakring Impeller

```
C  program R103 simulates flow of rock through port of "BREAKRING"
C  device having curved walls.
C  as R102 but does not include variables description for detached
C  condition.
C
      REAL ENDPTS(500,2),MIDPTS(500,2),S(500),SS(500),R(500),
     &ANG(500),RHO(500),ALPHA(500)
C
      READ(5,*)NOPTS,((ENDPTS(I,1),ENDPTS(I,2)),I=1,NOPTS),AV,XMU,U
C
      NOSEGS=NOPTS-1
      V2=U
C
      DO 1 I=1,NOSEGS
C
C  S(I) :segment length
C  SS(I):sum of segment lengths
C
      SX=ENDPTS(I+1,1)-ENDPTS(I,1)
      SY=ENDPTS(I+1,2)-ENDPTS(I,2)
      S(I)=SQRT(SX*SX+SY*SY)
      IF(I.EQ.1)THEN
        SS(I)=S(I)
        ELSE
          SS(I)=SS(I-1)+S(I)
          ENDIF
C
C  MIDPTS(I,1):segment midpoint,x-coordinate
C  MIDPTS(I,2):segment midpoint,y-coordinate
C  R(I)       :radius from port axis to segment midpoint
C  ANG(I)     :angle between radius and x-axis
C  RHO(I)     :angle between segment tangent and x-axis
C  ALPHA(I)   :angle between segment tangent and radius
C
      MIDPTS(I,1)=(ENDPTS(I,1)+ENDPTS(I+1,1))/2
      MIDPTS(I,2)=(ENDPTS(I,2)+ENDPTS(I+1,2))/2
      R(I)=SQRT(MIDPTS(I,1)**2+MIDPTS(I,2)**2)
      XMX=MIDPTS(I,1)
      YMY=MIDPTS(I,2)
      IF((YMY.GT.0).AND.(XMX.LT.0))THEN
      ANG(I)=3.14159-ATAN(-YMY/XMX)
      ELSEIF((YMY.LT.0.).AND.(XMX.LT.0.))THEN
      ANG(I)=3.14159+ATAN(YMY/XMX)
      ELSE
      ANG(I)=ATAN(YMY/XMX)
      ENDIF
      DY=ENDPTS(I+1,2)-ENDPTS(I,2)
      DX=ENDPTS(I+1,1)-ENDPTS(I,1)
      IF((DY.GT.0).AND.(DX.LT.0))THEN
      RHO(I)=3.14159-ATAN(-DY/DX)
      ELSEIF((DY.LT.0.).AND.(DX.LT.0))THEN
      RHO(I)=3.14159+ATAN(DY/DX)
      ELSE
      RHO(I)=ATAN(DY/DX)
      ENDIF
      ALPHA(I)=RHO(I)-ANG(I)
    1 CONTINUE
C
      WRITE(6,*)'AV=',AV,'rads/s'
      WRITE(6,*)'MU=',XMU

      WRITE(6,10)
C
      I=0
    3 I=I+1
      V1=V2
      IF(V1.LT.0.)THEN
        WRITE(6,17)ENDPTS(I,1),ENDPTS(I,2)
        WRITE(6,18)
        GOTO 6
        ELSE
        ENDIF
      WRITE(6,11)ENDPTS(I,1),ENDPTS(I,2),V1
      FNA= AV*AV*R(I)*SIN(ALPHA(I))
      FNB= 2*AV*V1
      FNC= V1**2*SIN(RHO(I+1)-RHO(I))/S(I)
      FN1 = FNA+FNB+FNC
      FF2= XMU*FN1
      AP1 = AV*AV*R(I)*COS(ALPHA(I))-FF2
      V2S = V1**2+2*AP1*S(I)
      IF ( V2S.LT.0.) THEN
      WRITE (6,19)
      GOTO 6
      ELSE
      END IF
      V2 = SQRT(V2S)
      IF(FN1.LT.-0.01)THEN
          CALL PATH(ENDPTS,MIDPTS,RHO,I,V1,V2,S,SS,NOPTS,ITATUS,R,AV,
     &     ANG)
          ELSE
            WRITE(6,12)MIDPTS(I,1),MIDPTS(I,2),S(I),SS(I),AP1,FN1,FF2
            ENDIF
      IF(I.LT.NOSEGS)THEN
        GOTO 3
        ELSE
          ENDIF
      IF(ITATUS.EQ.1)THEN
      WRITE(6,20)
      WRITE(6,17)ENDPTS(NOPTS,1),ENDPTS(NOPTS,2)
        ELSE
        WRITE(6,11)ENDPTS(NOPTS,1),ENDPTS(NOPTS,2),V2
        ENDIF
```

```
C
   10 FORMAT(1H ,T3,'COORDS(m)',T25,'S(m)',T40,'SS(m)',T55,'V(m/s)',
     &T70,'AP(m/s**2)',T85,'FN(N)',T100,'FF(N)')
   11 FORMAT(1H ,T3,G12.6,T12,G12.6,T55,G12.6)
   12 FORMAT(1H ,T3,G12.6,T12,G12.6,T25,G12.6,T40,G12.6,T70,G12.6,
     &T85,G12.6,T100,G12.6)
   17 FORMAT(1H ,T3,G12.6,T12,G12.6)
   20 FORMAT(1H ,T3,'particle detached from surface')
   18 FORMAT(1H ,T3,'velocity reversed')
C
    6 STOP
      END
C
      SUBROUTINE PATH(ENDPTS,MIDPTS,RHO,I,V1,V2,S,SS,NOPTS,ITATUS,R,
     &AV,ANG)
      REAL ENDPTS(500,2),MIDPTS(500,2),RHO(500),S(500),SS(500),R(500)
      REAL ANG(500)
      WRITE(6,14)
      WRITE(6,15)MIDPTS(I,1),MIDPTS(I,2),S(I),SS(I)
C
C   VX1         :absolute x- speed     after separation
C   VY1         :absolute y- speed     after separation
C   THETA       :angle between absolute trajectory and x-axis
C
      VX1=V1*COS(RHO(I))-AV*ENDPTS(I,2)
      VY1=V1*SIN(RHO(I))+AV*ENDPTS(I,1)
      IF((VY1.GT.0).AND.(VX1.LT.0))THEN
      THETA=3.141592654-ATAN(-VY1/VX1)
      ELSE IF((VY1.LT.0).AND.(VX.LT.0))THEN
      THETA=3.141592654+ATAN(VY1/VX1)
      ELSE
      THETA=ATAN(VY1/VX1)
      ENDIF
      DO 2 K=I+1,NOPTS-1
      VI=SQRT(VX1*VX1+VY1*VY1)
      TIMEA=VI*VI
      TIMEB=2*VI*(ENDPTS(I,1)*COS(THETA)+ENDPTS(I,2)*SIN(THETA))
      TIMEC=ENDPTS(I,1)**2+ENDPTS(I,2)**2-R(K)**2
      TIME=(SQRT(TIMEB*TIMEB-4*TIMEA*TIMEC)-TIMEB)/(2*TIMEA)
C
      YI=ENDPTS(I,2)+VI*SIN(THETA)*TIME
      XI=ENDPTS(I,1)+VI*COS(THETA)*TIME
      IF((YI.GT.0).AND.(XI.LT.0))THEN
      GAMMA=3.141592654-ATAN(-YI/XI)
      ELSE IF((YI.LT.0).AND.(XI.LT.0))THEN
      GAMMA=3.141592654+ATAN(YI/XI)
      ELSE
      GAMMA=ATAN(YI/XI)-AV*TIME
      ENDIF
      IF(GAMMA.LT.ANG(K))THEN
      VABS=SQRT((VY1-AV*XI)**2+(VX1+AV*YI)**2)
      IF(((VY1-AV*XI).GT.0).AND.((VX1+AV*YI).LT.0))THEN
      BETA=3.141592654-ATAN((AV*XI-VY1)/(VX1+AV*YI))
      ELSEIF(((VY1-AV*XI).LT.0).AND.((VX1+AV*YI).LT.0))THEN
      BETA=3.141592654+ATAN((VY1-AV*XI)/(VX1+AV*Y1))
      ELSE
      BETA=ATAN((VY1-AV*XI)/(VX1+AV*YI))
      ENDIF
      XANG=RHO(K)+AV*TIME-BETA
           IF(XANG.GE.0)THEN
           V2=VABS*COS(XANG)
           WRITE(6,18)VABS,XANG
           GOTO 21
           ELSE
           WRITE(6,19)VABS,XANG
           WRITE(6,17)ENDPTS(K,1),ENDPTS(K,2)
           WRITE(6,15)MIDPTS(K,1),MIDPTS(K,2),S(K),SS(K)
           ENDIF
      ELSE
      WRITE(6,20)
      WRITE(6,17)ENDPTS(K,1),ENDPTS(K,2)
      WRITE(6,15)MIDPTS(K,1),MIDPTS(K,2),S(K),SS(K)
      ENDIF

    2 CONTINUE
      ITATUS=1
   14 FORMAT(1H ,T3,'particle detaches from surface')
   15 FORMAT(1H ,T3,G12.6,T12,G12.6,T25,G12.6,T40,G12.6)
   16 FORMAT(1H ,T3,'particle strikes port tip'
     &/T3,'impact speed',G12.6,'m/s')
   17 FORMAT(1H ,T3,G12.6,T12,G12.6)
   18 FORMAT(1H ,T3,'particle reattaches to surface'
     &/T3,'impact speed ',G12.6,'m/s impact angle',G12.6,' rads')
   19 FORMAT(1H ,T3,'particle strikes surface prominence,'
     &/T3,'impact speed ',G12.6,'m/s impact angle',G12.6,' rads')
   20 FORMAT(1H ,T3,'particle detached from surface')
   21 I=K-1
      RETURN
      END
```

8. BIBLIOGRAPHY

1. Bartley, Bryan A. (1989) Developments in the Barmac vertical shaft impactor design. Quarry Management. July.

2. Eck, Bruno (1973) Fans. 4th ed. Pergamon Press. London.

3. Garland, Paul A. (1977) "Machine for comminuting materials" (patent application). Elkington and Fife, Chartered Patent Agents. London.

4. Garland, Paul A. (1983) "A Design Study for an Improved Comminution Machine for Brittle Materials, of the Impact Breaker Type". Garland Designers and Engineers.

5. Harvey, Alan (undated) "Impact Crushing". Peabody Holmes Ltd. London.

6. Hewitt-Robins Incorporated (undated) "Crushers and Crushing Plants".

7. Higginson, Gordon R. (1974) Foundations of Engineering Mechanics. Longman. London.

8. Hill, H.E. (1987) Energy saving in vertical shaft impactors. Mine and Quarry. December.

9. Höffl, Karl (1985) Zerkleinerungs- und Klassiermaschinen. VEB Deutscher Verlag für Grundstoffindustrie. Leipzig.

10. Huwald (1987) Impact crushing practice. Quarry Management. January.

11. Johnston, R.L. (1982) TEAPACK Users' Manual. Mathematical Subroutines for Numerical Methods. University of Toronto. John Wiley and Sons. New York.

12. Landwehr, D. and Pahl, M.H. (1987) Comminution processes in a turbo-mill-Part 1. Aufbereitungs-Technik- Nr. 2.

13. Müller, G. and Weigl, T. (1988) Use of vertical impact crushers as an alternative to conventional comminution processes. Aufbereitungs-Technik-Nr. 1.

14. Prior, W.A.J. (1985) GHOST-80 User Manual. UKAEA Culham Laboratory.

15. Settles, Gary S. (1986) Modern Developments in Flow Visualisation. AAIA Journal. Volume 24.